Science of the Total Environment 804 (2022) 149983

Contents lists available at ScienceDirect

Science of the Total Environment

journal homepage: www.elsevier.com/locate/scitotenv

Microphytobenthos spatio-temporal dynamics across an intertidal gradient using Random Forest classification and Sentinel-2 imagery

S. Haro [a,*], B. Jesus [b], S. Oiry [b], S. Papaspyrou [a], M. Lara [a], C.J. González [c], A. Corzo [a]

[a] Department of Biology, Faculty of Marine and Environmental Sciences, University of Cadiz, 11510 Puerto Real, Cadiz, Spain
[b] Université de Nantes, Faculté des Sciences, Mer-Molécules-Santé (MMS), RSBE, EA2160 Nantes, France
[c] Division of Naval Support and Oceanography, Marine Hydrographic Institute, Spanish Navy, 11007 Cadiz, Spain

HIGHLIGHTS

- Random forest applied to Sentinel-2 images allowed mapping intertidal communities.
- A bathymetry map was developed combining remote sensing, *in situ* data and modelling.
- Four-year microphytobenthos spatio-temporal dynamics were monitored by remote sensing.
- MPB cover, biomass and net growth rates showed seasonal and interannual changes.
- MPB cover, biomass and net growth rate patterns differed with sea level gradient.

GRAPHICAL ABSTRACT

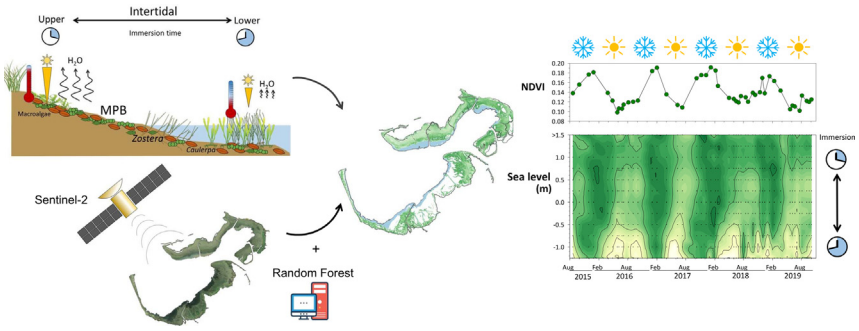

ARTICLE INFO

Article history:
Received 1 May 2021
Received in revised form 7 July 2021
Accepted 24 August 2021
Available online 28 August 2021

Editor: José Virgílio Cruz

Keywords:
Remote sensing
Machine learning
Biomass
Benthic microalgae
Seagrass
Intertidal gradient

ABSTRACT

Microphytobenthos (MPB) provides important ecosystem functions and services, contributing significantly to the total primary production in shallow coastal ecosystems. However, determining the factors that regulate the seasonal changes of MPB and its distribution patterns at larger scales is hindered by the considerable spatial and temporal variability in these environments. Here, we studied the dynamics of intertidal MPB biomass, cover, and net growth rates in a south European tidal flat (Cadiz Bay, Spain) over a four-year period using the Normalized Difference Vegetation Index (NDVI) calculated from Sentinel-2 satellite images. Pixels dominated by different benthic communities (MPB, *Zostera sp.*, *Caulerpa* sp. and green macroalgae) were identified at a 10-m resolution using a Random Forest (RF) machine learning classification algorithm. MPB dominated the intertidal zone. MPB cover did not show a clear seasonal pattern and was clearly higher in the middle of the intertidal range of sea level. Despite interannual variability, MPB biomass was always higher during winter, coinciding with observations from other low latitude intertidal flats with temperate climate, and in the upper-middle intertidal. Net rates of MPB biomass change, calculated from the differences in MPB NDVI over time, showed maximal net growth rates from autumn to winter and maximum loss rates during spring and summer, although with high variability. Our study demonstrates that RF algorithms allow mapping MPB and other intertidal communities from Sentinel-2 multispectral satellite imagery accurately obtaining invaluable information from large areas at very high spatio-temporal resolution. The dissimilarities observed in the patterns of MPB variables over time or sea level, indicate differences in their ecological regulation, still largely unknown both here and in other temperate

* Corresponding author.
E-mail addresses: sara.haro@uca.es (S. Haro), bruno.jesus@univ-nantes.fr (B. Jesus), simon.oiry@univ-nantes.fr (S. Oiry), sokratis.papaspyrou@uca.es (S. Papaspyrou), miguel.lararayo@uca.es (M. Lara), carlosjose.gonzalez@uca.es (C.J. González), alfonso.corzo@uca.es (A. Corzo).

https://doi.org/10.1016/j.scitotenv.2021.149983

climate intertidal flats. High resolution remote sensing can aid in their detailed and systematic study producing a more integrated view of these systems and contributing to their science-based management and conservation.

1. Introduction

Intertidal flats can contribute significantly to total production in coastal areas (Underwood and Kromkamp, 1999). A large part of this production (up to 50% of the total benthic community) can be due to microphytobenthos (MPB) (Asmus and Asmus, 2000; Haro et al., 2020; Frankenbach et al., 2020), *i.e.* the photosynthetic community that inhabits the sediment photic layer (μm to mm), comprising of diatoms, cyanobacteria and green microalgae. MPB provides important ecosystem functions such as being a food source for higher trophic level organism, of high economic value (*e.g.* fish, shellfish), mediating nutrient and oxygen exchanges across the sediment-water interface and acting as natural CO_2 sinks (Day et al., 1990; Jimenez-Arias et al., 2020; Lebreton et al., 2019); thus playing an important biogeochemical role in these ecosystems (Canfield et al., 2005; MacIntyre et al., 1996). Moreover, MPB diatoms excrete large amounts of extracellular polysaccharides which serve as a carbon source for heterotrophic bacteria (Bohórquez et al., 2017; Underwood et al., 1995) and increase the cohesion of the sediment surface, contributing to their stabilization and reducing their erosion rates (Paterson, 1989; Yallop et al., 1994). Therefore, MPB is an important component of coastal shallow ecosystems, whose distribution and variation in both abundance and production allows to assess the state of the ecosystem functions including water quality (Barinova et al., 2019; Oiry and Barillé, 2021).

Traditionally, studies on the dynamics of MPB biomass, either *in situ* or in the laboratory, have been performed using techniques such as pulse amplitude modulation (PAM) fluorescence techniques, spectral reflectance (on the surface or microprofiles), or spectrophotometric chlorophyll analysis (*e.g.* Jesus et al., 2005; Kühl et al., 1994; Serôdio et al., 2006). However, these methods are difficult to upscale in order to monitor large intertidal areas. Currently there is an increased interest in remote sensing studies, which allow studying MPB biomass dynamics at high temporal and spatial resolutions, eliminating the difficulties related to *in situ* sampling and related costs (Benyoucef et al., 2014; Brito et al., 2013; Van der Wal et al., 2010). Most studies use the Normalized Difference Vegetation Index (NDVI) as a proxy of microphytobenthic chlorophyll-*a* (MPB Chl-*a*), with NDVI estimated from different multispectral satellite images *e.g.* SPOT (Benyoucef et al., 2014; Brito et al., 2013), aqua MODIS (Savelli et al., 2018; Van der Wal et al., 2010) or Landsat (Daggers et al., 2018; Echappé et al., 2018). Microphytobenthic NDVI (MPB NDVI) is often transformed to MPB Chl-*a* to show MPB biomass maps, although the real MPB biomass could be over- or underestimated during the transformation process due to issues related to Chl-*a* depth distribution inside the sediment (Jesus et al., 2006). Recent studies have analysed satellite multispectral images by means of classified or unclassified supervision to map intertidal vegetation and salt marshes (Casal et al., 2011; Li et al., 2010; Van der Wal et al., 2014). Among these techniques, Random Forest (RF) algorithm is a machine learning classification method that can be trained to classify different datasets in classes or categories (Luo and Wang Xinhui Liu, 2018; Niculescu et al., 2018; Oiry and Barillé, 2021). The spatial, spectral and temporal resolutions of available satellite images are important features to be considered. So far, most MPB related studies have depended on satellite images with relatively low spatial resolution, in the range of 20 × 20 m for SPOT (Benyoucef et al., 2014; Brito et al., 2013), 30 × 30 m Landsat (Daggers et al., 2018; Echappé et al., 2018) and 250 × 250 m for MODIS (Savelli et al., 2018; Van der Wal et al., 2010). However, most recent satellites, such as the Sentinel-2A and Sentinel-2B multispectral satellites (launched June 2015 and March 2017, respectively) have higher-resolution optical imagery, down to 10 m × 10 m pixel size, 13 spectral bands and fly over the same area every 2 - 5 days depending on latitude. The increased re–visiting time is particular important when investigating tidal flats because it increases the chances of acquiring satellite images synchronized with low tide. Very recently, these satellites have been used for the first time to investigate several aspects of MPB ecology and confirm that higher spatio-temporal and multispectral resolutions are powerful tools to study MPB spatio-temporal dynamics in detail (Daggers et al., 2020; Oiry and Barillé, 2021; Zhang et al., 2021).

MPB distribution patterns in the intertidal zones can be very variable due to the fact that MPB abundance depends on several environmental factors, such as irradiance, temperature, sediment type, tidal height, sediment desiccation, grazing pressure, salinity, topography, and nutrients availability both in the sediment porewater and the water column (Bohórquez et al., 2019; Jesus et al., 2006, 2009; Savelli et al., 2018). Fluctuations in any of these variables can result in changes of MPB biomass on spatio-temporal scales ranging from days to years (Migné et al., 2004; Serôdio et al., 2005) and from centimetres to kilometres (Guarini et al., 1998; Jesus et al., 2005; Orvain et al., 2012). Some of these ecological factors are more conditioned by season, typically irradiance and temperature, being likely the main responsible of MPB seasonal changes (Benyoucef et al., 2014; Brito et al., 2013; Migné et al., 2004); while others are more related to environmental heterogeneity, *i.e.* sediment grain size, bathymetry and topography and (Haro et al., 2020; Kwon et al., 2020; Van der Wal et al., 2010). Despite this environmental heterogeneity, MPB biomass has been found to be higher in the upper intertidal zone and to decrease seawards in northern (Benyoucef et al., 2014; Van der Wal et al., 2010), and southern European estuaries (Brito et al., 2013; Orvain et al., 2012), suggesting that the position of MPB in the sea level intertidal range (SL) could be a major ecological driver for MPB standing stocks. The position of a given sediment area in the SL range is one of the major geomorphological characteristics defining intertidal ecotopes, i.e. areas with similar geomorphological and hydrodynamics characteristics, silt contents and elevations, which form relatively constant ecological environments within the intertidal zone, being suitable for specific benthic communities (Baptist et al., 2019; Bouma et al., 2005). Changes in SL affect directly a number of environmental variables like emersion time, daily irradiance dose, mean daily sediment temperature, and even the period in which different marine organisms can graze on MPB; all potentially key variables determining MPB biomass, cover and primary production dynamics. However, information confirming the universality of the MPB biomass patterns along the intertidal gradient in different coastal ecosystems is still limited. Additionally, no information exists on what the patterns of MPB cover and MPB growth rates are or how MPB distribution along the SL gradient changes with season. Seasonal distribution of MPB biomass seems to differ between northern and southern European estuaries. In northern Europe, the maximum of MPB biomass is often observed in summer (Van der Wal et al., 2010), whereas in southern Europe, in most cases, the maximum is found in winter and early spring (Brito et al., 2013; Garcia-Robledo et al., 2016; Haro et al., 2020; Savelli et al., 2018). Testing the generality of this latitudinal pattern by *in situ* field studies is difficult and time consuming due to the high MPB environmental heterogeneity and patchiness at different spatial scales. However, high resolution remote sensing in combination with RF classification can be a powerful tool to map the seasonal changes in MPB biomass, cover and net growth rate, taking into account the spatial heterogeneity of the intertidal environment at different scales.

In the present study, we investigated the spatio-temporal dynamics of MPB biomass, cover and growth rates along the SL gradient. We used Sentinel-2 multispectral images acquired at around low tide from mid-2015 to 2019 and a RF machine learning classification method to determine MPB spatial–temporal dynamics in a Southern European shallow bay (inner Cadiz Bay, SW Spain), where MPB coexists with seagrass meadows, *e.g. Zostera* sp. and *Cymodocea sp.,* and macroalgae, such as *Ulva* sp. and *Caulerpa* sp. Our specific aims were: (1) to classify the intertidal primary producers communities using a RF algorithm; (2) to test the hypothesis that the highest MPB biomass would be found at the upper intertidal zone; (3) to test the hypothesis that the maximum MPB biomass would occur in winter and early spring; (4) investigate if observed patterns were uniform across the entire studied area; and (5) to estimate MPB net growth rates to explore the factors that might affect the observed spatio-temporal patterns.

2. Material and methods

2.1. Study site

The inner Cadiz Bay is a shallow water body located in South-Western Spain (36°29'52.9"N; 6°12'49.7"W), with an area of ~36 km^2, a semi-diurnal tidal regime and maximum depth of ~3.5 m relative to the local mean sea level (MSL) (Fig. 1). The intertidal zone covers 60% of the inner bay surface (Sanchez De Lamadrid Rey and Muñoz Pérez, 1994). A significant part of this surface is covered by *Zostera noltei* meadows, sediments colonised by MPB and occasionally by green macroalgae (Garcia-Robledo et al., 2012; Lara et al., 2012). The infralittoral region is dominated by *Caulerpa prolifera* and to a lesser extent *Cymodocea nodosa* meadows (Egea et al., 2019; Gómez Ordoñez, 2008; Haro et al., 2020; Lara et al., 2016).

2.2. Sentinel-2 data processing

All Sentinel-2 images were downloaded from Copernicus Open Access Hub. A total of 49 multispectral images of inner Cadiz Bay were selected from 2015 to 2019. Selected images (Supplementary Table 1) were acquired during cloud free conditions (<10%) and within a maximum of two hours from low tide. Sentinel-2 satellite images can have a high spatial resolution, down to 10 m × 10 m pixel size. However, the spatial resolution is dependent on the spectral bands used: 10 m for B2 (490 nm), B3 (560 nm), B4 (665 nm) and B8 (842 nm) bands; 20 m for B5 (705 nm), B6 (740 nm), B7 (783 nm), B8a (865 nm), B11 (1610 nm); and B12 (2190 nm) bands and 60 m for B1 (443 nm), B9 (940 nm) and B10 (1375 nm) bands. All Sentinel-2A images (level of correction 1C), from June-2015 to March-2017, were corrected for atmospheric effects using the SEN2COR tool (SEN2COR, n.d.), which was available within Sentinel Application Platform (SNAP) toolbox. Sentinel -2A and Sentinel-2B images (level of correction 2Ap and 2A), from April-2017 to October-2019, were used directly. Scenes were registered in WGS 84/UTM zone 30 N coordinate system (EPSG: 32630) and the intertidal zone was masked using a Geographical Information System software (QGIS, https://www.qgis.org). The intertidal area was selected by excluding water pixels using the Normalized Difference Water Index (NDWI) (Li et al., 2013; McFeeters, 1996): NDWI = [band 3- band 8]/[band 3 + band 8], where band 3 was green and band 8 was Near Infra-Red (NIR). We used an image acquired at high tide to determine the upper limit of the intertidal area and an image acquired at low tide to determine the lower limit; both images were acquired at spring tides with the highest tidal coefficients we observed. The difference between the two images corresponded to the maximum intertidal surface we could estimate. This surface is slightly underestimated since the mean lower sea levels observed in spring tides in the inner bay of Cadiz are about −1.6 m SL and our data reach up to −1.4 m.

2.3. Random Forest

The intertidal zone was classified using the Random Forest method (RF, Breiman, 2001), which is a machine learning method combining decision trees and bootstrapping. It uses supervised classification algorithms to handle collinearity and non-linearity between predictive variables. Each decision tree is created using a random sample of predictive data resampled by bootstrapping at each iteration of the algorithm. Then for each pixel, the final classification is obtained by a majority vote, i.e. the class that appeared most often at the end of each algorithm iteration. This classification method can be divided into 3 stages: model building, image classification and the estimation of model accuracy.

2.3.1. RF model building

To build an RF model, *in situ* field data are used as training data by the RF algorithm. Thus, *in situ* data were collected by Haro et al. (2020), creating waypoints where different types of benthic substrates

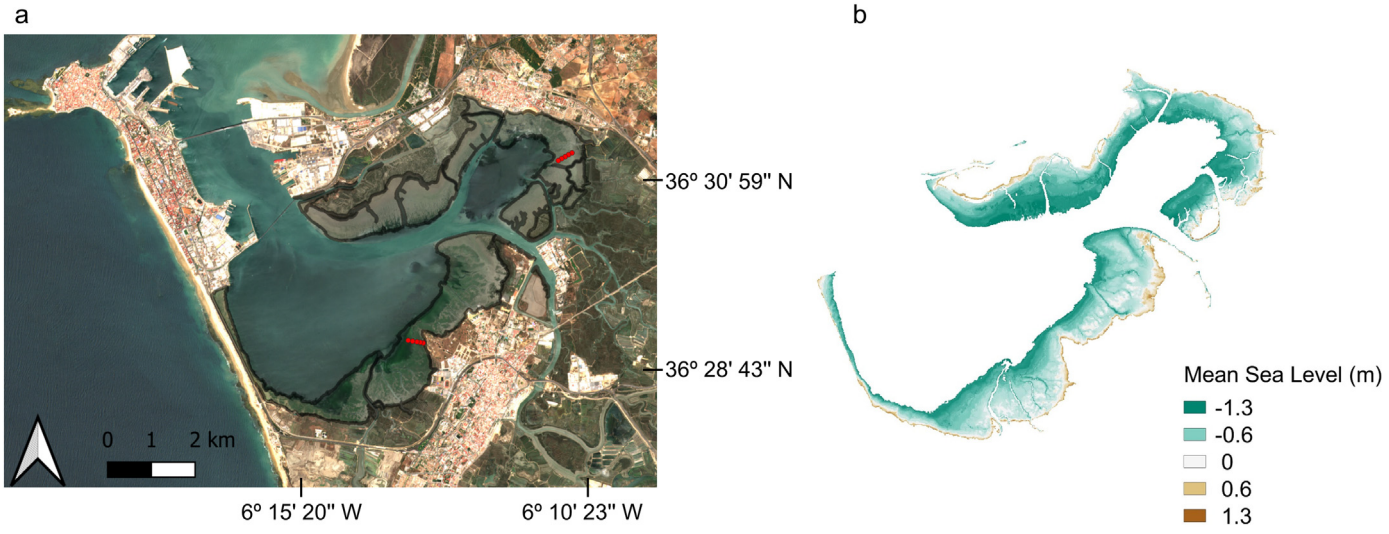

Fig. 1. (a) Sentinel-2 satellite image of the inner Cadiz Bay (SW Spain, South Europe). The black line delimits the intertidal zone. *In situ* measurements of microphytobenthic biomass (Chl-*a*) were done along the intertidal gradient at two sites (red points). (b) Map of sea level (SL, m) in the intertidal area. The spatial resolution of the SL layer was 10 × 10 m.

were observed. The different types of primary producers communities observed were: green macroalgae (mainly *Ulva sp.*), *Zostera sp.*, *Caulerpa* sp. and sediment colonised with MPB. All these points were created using a GPS "Garmin etrex Legend" with a spatial accuracy of 15 m. In total, five classes were created using field data (green macroalgae, *Caulerpa*, MPB, *Zostera*, and water). In parallel, a Sentinel-2 image was acquired on the 27th of May 2016 to obtain reflectance data for each sampling point. The creation of the model was realized using the "caret" package (Kuhn et al., 2018) for R software (R Core Team, 2017). The parameter number of trees (n_{tree}) was set to 500 (Oiry and Barillé, 2021). All 10 and 20 m (spatially resampled at 10 m) Sentinel-2 bands were used as predictors, as well as the Normalized Difference Vegetation Index (NDVI), the Atmospherically Resistant Vegetation Index (ARVI), the Modified Chlorophyll Absorption Ratio Index (MCARI) and the Normalized Different Water Index (NDWI) (Daughtry et al., 2000; Kaufman and Tanré, 1992; McFeeters, 1996; Rouse et al., 1973). The parameter number of features in each split (m_{try}) was kept at the default value of the caret package: mtry $= \sqrt{p}$, where p is the number of predictor variables (14 in this case).

2.3.2. RF classification and accuracy assessment

The Random Forest (RF) classification was also made using the "caret" package (Kuhn et al., 2018). The RF model was used to classify intertidal pixels of 49 Sentinel-2 images (10 m resolution). The number of pixels of each class was used to estimate the surface covered by each class. A validation dataset was created from photo interpretation of the study site (111 points with a resolution of about 100 m^2) and was used to estimate the accuracy of the classification on a Sentinel-2 images acquired the 27th of May 2016, 6th of July 2016, 4th of October 2016, 2nd of January 2017 and 2nd of April 2017, months at which *in situ* samplings were carried out along intertidal gradient in inner Cadiz bay (Supplementary Table 2). The error matrix of this model was built according to Congalton (1991). Each cell of this matrix represents the number of classified pixels, where rows present the RF classified data and columns are training data. The intersection between rows and columns with the same name are the correctly-classified pixels. Three metrics were used to evaluate the accuracy of the classification. The overall accuracy of the model is the ratio of correctly-classified pixels to the sum of all pixels used as reference in the error matrix. The producer's accuracy of each class is the ratio of correctly classified pixels to the total number of validation pixels of the same class. Finally, the user's accuracy is the number of correctly classified pixels in one class divided by the number of pixels classified in the same class (Oiry and Barillé, 2021).

2.4. NDVI data processing

NDVI values were calculated for all pixel classes using surface reflectance in the near-infrared (band 8) and red (band 4) as: NDVI = [band 8 – band 4]/[band 8 + band 4] (Rouse et al., 1973). NDVI values of pixels classified by RF as MPB (MPB NDVI) were used to characterise the MPB community at the ecosystem scale using three proxies: (1) changes in MPB biomass, estimated from NDVI value (NDVI $pixel^{-1}$); (2) changes in MPB cover as percentage of pixels classified as MPB with respect to total number of pixels; and (3) changes in MPB net growth and loss rates estimated from the differences in NDVI for the same pixel location between successive satellite images. MPB NDVI and *in situ* MPB Chl-*a* concentration, measured in two transects done in the inner Bay of Cadiz in July and October, in 2016, and in January and April, in 2017 (Haro et al., 2020), showed a statistically significant exponential relationship ($r^2 = 0.45$; $n = 24$; $p < 0.05$; Supplementary Fig. 1). However, we decided to use directly the intensity of NDVI per pixel as a proxy of MPB biomass without further transformation to Chl-*a* to reduce potential estimation errors.

Net growth rates of MPB standing stocks (μ_{NDVI}, day^{-1}) were calculated from the differences in MPB NDVI for the same pixel between two successive images, $NDVI_{t+1}$, obtained at time t + 1, and $NDVI_t$, obtained at time t, according to eq. 1.

$$\mu_{NDVI} = \frac{Ln\ NDVI_{t+1} - Ln\ NDVI_t}{(t+1) - t} \quad (1)$$

2.5. MPB biomass along sea level intertidal gradients

The average MPB biomass, expressed in mean NDVI $pixel^{-1}$, and MPB cover (% of pixels classified as MPB) with respect to sea level (SL) in the intertidal area of inner Cadiz bay were measured using QGIS "Zonal statistics" plugin. The topography of the intertidal areas in relation to MSL was established at a 10 m spatial resolution. This grid was calculated by estimating a relationship between multiple water-land boundaries (established by NDWI from Sentinel-2 data) and water height data from tide-gauges deployed by the Spanish Marine Hydrographic Institute (armada.defensa.gob.es/ihm) in Cadiz Bay, following the methodology described by (Bishop-Taylor et al., 2019). The supratidal topography was completed by the 5 m resolution digital elevation model of the Spanish National Geographic Institute (www.ign.es). The obtained product covers almost the entire inner Cadiz Bay intertidal area, with the exception of a deeper low-slope flat on the eastern part, which only emerges at the lowest astronomical tides. The resolution of the SL vectorial layer was 10 × 10 m. Squared buffers of 5 m were created around SL points to extract the biomass of MPB and other intertidal communities in the 49 acquired images. SL intervals of 25 cm along intertidal gradient in inner Cadiz Bay were then determined to study spatial patterns of MPB biomass and cover. MPB growth rates were also calculated along the intertidal gradient of SL according to the previous equation.

2.6. Meteorological data

Meteorological data temporal series were analysed from to 2015 to 2019. Meteorological values were averaged for the week before each available satellite image to investigate their possible effect on MPB. Meteorological conditions (air temperature, wind speed and rainfall) were obtained from the closest Junta de Andalucía meteorological station, located in El Puerto de Santa Maria, about 10 km from the inner bay. Monthly average of air temperature showed a typical seasonal pattern of temperate climates with higher values in August (25 °C) and lower in January (13 °C). The average wind speed oscillated between 5.21 and 18.66 km h^{-1}, in February and September of 2018 respectively. Overall, rainfall was higher in winter with maximum accumulated rainfall (previous 7 days) of 0.18 mm in 2019 (Supplementary Fig. 2).

2.7. Statistical analysis

Seasonal changes in the mean MPB biomass, calculated for every one of the 49 Sentinel-2 images, were tested by Two-way ANOVA with mixed linear effects. Thereafter, Tukey Contrasts tests were applied (Bonferroni method; adjusted p values <0.05). Coefficients of variation (CV) were also calculated from MPB NDVI maps to study MPB biomass spatial–temporal variability along the intertidal gradients. Changes in mean MPB NDVI for the inner bay with time were fitted using Microsoft Excel 2016 Solver to a general sine wave equation (eq. 2; Mansfield and Sanith, 1984; Haro et al., 2019),

$$MPB\ NDVI = A \sin\left(\frac{2\pi}{p}(t - s_t)\right) + b \quad (2)$$

where t is the independent variable time, in days elapsed from the first image date, A is the amplitude of oscillation, p is the period, s_t is the phase shift in time and b is the average MPB NDVI value.

3. Results

3.1. Intertidal communities of inner Cadiz bay classified by RF

Global accuracy of the RF model (*i.e.* the ratio of correctly-classified pixels to total number of validation pixels) was 80%. User's accuracy (*i.e.* the number of correctly classified pixels of a given class divided by the number of pixels classified in the same class by RF) was higher than 72% for all categorized classes, except for *Zostera sp.* (59%). Producer's accuracy (*i.e.* the ratio of correctly classified pixels to the total number of validation pixels of the same class) was higher than 75% for all categorized classes except green macroalgae (57%). In the case of sediment colonised with MPB, user's and producer's accuracies were 100% and 78% respectively, thus confirming that the RF algorithm used was adequate for monitoring MPB and its intertidal zonation (Table 1). The NDVI values corresponding to pixels classified as MPB were in the range of 0 - 0.45. NDVI values of *Zostera* sp. and macroalgae ranged between 0 and 1 and 0.16 - 0.61, respectively. The negative NDVI values generally corresponded to water and in some occasion to *Caulerpa sp.* (−0.61–1) (Supplementary Table 3).

Of the masked total intertidal area in inner Cadiz bay (13.07 km^2), the average surface covered by water in the 49 images was 2.5 ± 1.8 km^2 which corresponds to ~19% of the total intertidal area (Fig. 2). The percentage of water coverage depended on the tidal cycle and the specific time at which the satellite image was acquired. The presence of water prevents obtaining information about the benthic communities beneath it. Of the remaining emerged surface (81%), the mean surface classified as MPB was the highest (62%, 6.5 ± 1.1 km^2), followed by *Zostera sp.* (30%, 3.2 ± 1.0 km^2), *Caulerpa sp.* (6%, 0.7 ± 0.6 km^2), and other macroalgae (2%, 0.2 ± 0.2 km^2) (Fig. 2). Seasonal, spatial and interannual changes were observed in the area covered by different benthic communities (Fig. 2). The surface classified as MPB was higher at the north and northwest of the bay, where MPB was often the only primary producer growing along the intertidal gradient, while the area with the lowest MPB coverage was in the south-east (Fig. 2). Most pixels classified as *Zostera* sp. and *Caulerpa* sp. were located in the intertidal area of the south margin of the bay. In this zone, the pixels classified as MPB were usually distributed in the upper shore, *Zostera* sp. pixels were distributed in the intermediate shore, and *Caulerpa* sp. in the lower shore. The seasonal presence of green macroalgae in winter and the interannual variability in their cover was also clearly observed (Fig. 2).

3.2. Spatio-temporal patterns of MPB biomass and cover

MPB NDVI values were used as a proxy of *in situ* MPB Chl-*a* concentration (MPB biomass), expressed as NDVI $pixel^{-1}$, without further transformation to Chl-*a* units (Supplementary Fig. 1). MPB biomass decreased in spring and summer and increased in autumn, reaching its maximum in winter, showing a clear seasonal pattern (Figs. 3, 4). The average values of MPB biomass calculated for the entire inner Cadiz bay from every image showed a maximum in winter (Fig. 4a, b). These winter maxima in mean MPB biomass were significantly higher than mean values in spring and summer, but not from those of autumn ($F_{9,3} = 14.14$, $P < 0.001$; two-way mixed ANOVA and post-hoc comparisons with Tukey test, p values <0.05 adjusted by Bonferroni method). When the average MPB biomass was fitted to a periodic wave equation a periodic temporal pattern of 368 days was found (Supplementary Fig. 3). Seasonal pattern in MPB biomass presented a significant negative correlation with the mean air temperature (Pearson coefficient = −0.67; $n = 47$, $p < 0.05$) and mean wind speed (Pearson coefficient = −0.30; n = 47, p < 0.05) registered during the 7 days prior to the satellite image; while mean rainfall did not show any statistically significant relation with MPB biomass (Supplementary Fig. 2). In addition to the MPB NDVI seasonal pattern, interannual differences in the MPB NDVI range and in the spatial distribution were observed as well (Figs. 3, 4). MPB NDVI was generally higher and covered a larger area in the 2017´s winter than in 2018 and 2019´s winters, particularly in the south-west intertidal zones of the inner Cadiz bay (Fig. 3).

To further analyse MPB spatio-temporal distribution along the SL gradient, average values of MPB NDVI were calculated for different SL intervals for the entire inner bay and plotted against SL (Fig. 4). The seasonal pattern of MPB biomass and the interannual differences were highlighted when MPB NDVI was plotted against SL. Mean MPB biomass changed along the SL range, showing a clear seasonal pattern, with marked differences between winter and summer (Fig. 4a) and a general and significant trend to decrease with SL (Pearson coefficient = −0.90, $n = 12$; $p < 0.05$) (Fig. 4c). Although MPB biomass per unit of surface was higher in upper range of SL (SL > 0.5 m), the contribution of the MPB located in this upper SL range to the total intertidal MPB biomass of the inner bay was very low since this upper SL range represent a very small % of total intertidal area. Most of the intertidal area in inner Cadiz bay is located in a range of SL between +0.25 and −1 m (Fig. 4c). The importance of the SL for the seasonal and interannual variability in MPB biomass can be observed in the average coefficient of variation (CV) of MPB biomass along intertidal gradient (Supplementary Fig. 4a, c). Overall, the CV calculated for MPB biomass increased seawards, increasing 30% in the lower shore in comparison to the upper shore. High CV values were generally observed in late spring and summer while low values occurred mainly in winter, except in the 2018–2019 winter, were the annual minimum occurred later (Supplementary Fig. 4a, b).

In addition to changes in the relative amount of MPB biomass $pixel^{-1}$, remote sensing allowed to analyse the changes in the percentage of pixels of the intertidal zone classified as MPB (MPB cover). The average MPB cover for the entire intertidal zone oscillated between 18 and 56% over time (Fig. 5b). Changes in MPB cover with time did not show a clear seasonal pattern as the one found for MPB biomass. Thus MPB biomass and MPB cover were not significantly correlated (Pearson coefficient = −0.28, $n = 47$ $p < 0.05$). Moreover, the distribution of MPB cover along SL was more complex that the distribution of biomass $pixel^{-1}$ (Fig. 5c). MPB cover increased steeply seaward up to +0.5 m (upper shore), where the average maximum in MPB cover was located (~ 85%), a secondary maximum was positioned further seaward, at −0.5 m SL, decreasing strongly from this SL seaward (Fig. 5c). The secondary peak in MPB cover coincided roughly with a range of SL (−0.25 to −0.5 m) containing an important fraction of the intertidal area in inner Cadiz Bay.

3.3. Spatio-temporal changes in the MPB growth rate

Net increase rates of MPB standing stocks (μ_{NDVI}) presented evident spatial heterogeneity and interannual variability (Figs. 6, 7). The range

Table 1
Random Forest (RF) validation matrix to assess the accuracy of the classification procedure. The matrix was created based on *in situ* sampling (Haro et al., 2020) and visual inspection of RGB images and aerial photographs. Columns are classes observed *in situ* and rows are the result of RF classification. The intersection between columns and rows are correctly classified pixels. The intersection between producer and user's accuracy is the global accuracy of the RF model (Congalton, 1991).

	Water	Caulerpa	Zostera	Macroalgae	MPB	User's accuracy
Water	15	1	0	0	0	0.94
Caulerpa	0	16	0	0	6	0.73
Zostera	0	4	20	10	0	0.59
Macroalgae	0	0	0	13	1	0.93
MPB	0	0	0	0	25	1.00
Producer's accuracy	1.00	0.76	1.00	0.57	0.78	0.80

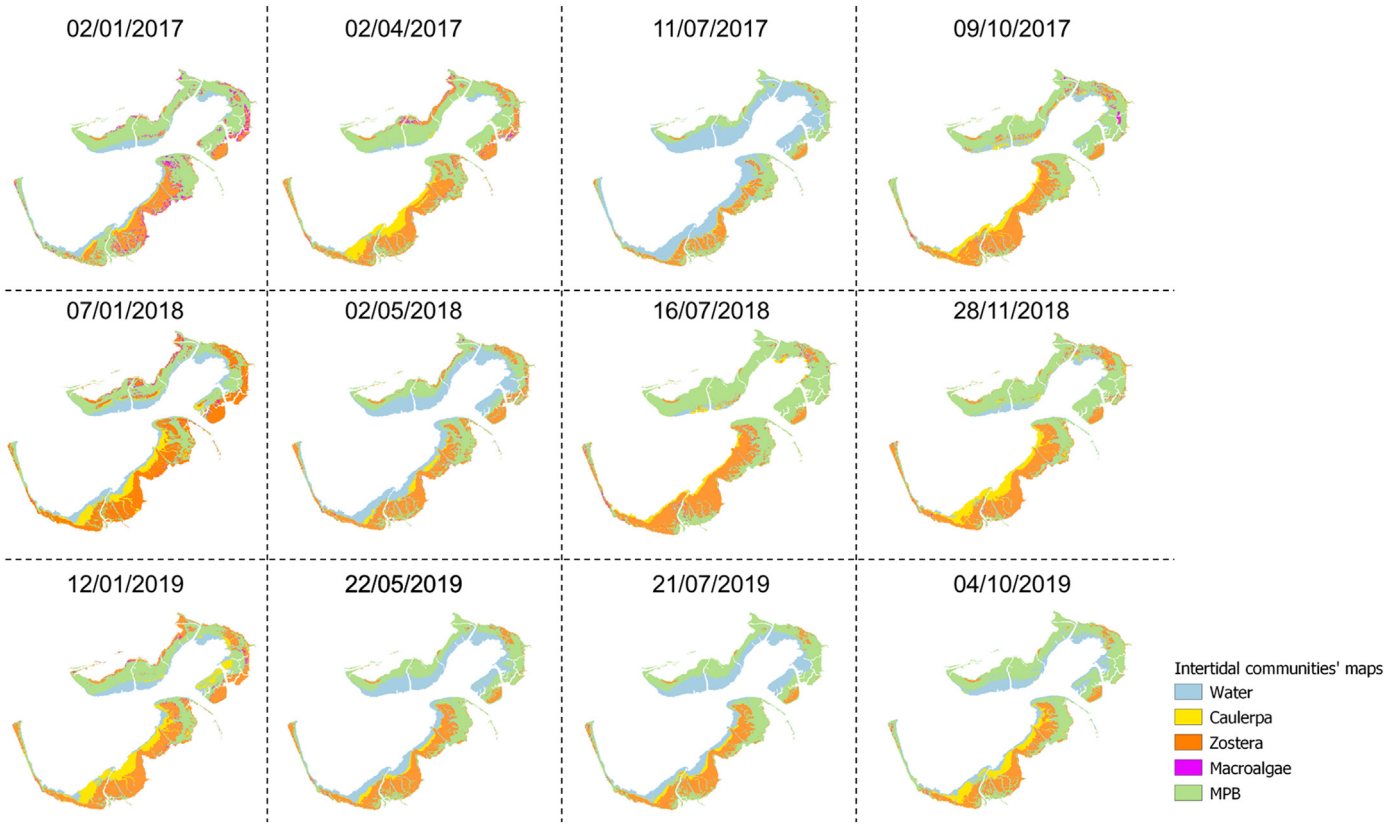

Fig. 2. Maps indicating the area occupied by the distinct primary producing communities considered in the intertidal area of inner Cadiz Bay, as determined using a Random Forest algorithm. Representative images of the four seasons (winter, spring, summer and autumn from left to right) are shown for three consecutive years (2017–2019). Pixels were classified as water, *Caulerpa sp.*, *Zostera sp.*, macroalgae and MPB by the Random Forest algorithm (see M&M).

of μ_{NDVI} generally oscillated from −0.047 to 0.077 d^{-1} (Fig. 6). More extreme positive and negative values of μ_{NDVI} ($> \pm 0.06$ d^{-1}) were observed when there were short time intervals between successive images, but these represented only 3.6% of the total analysed pixels (Fig. 7). MPB growing periods, where positive net growth rate (positive μ_{NDVI}) were observed, tended to occur mainly in autumn and early - mid winter (up to January - February), while from the end of winter, spring and summer, MPB biomass tended to decrease (negative μ_{NDVI}). However, in 2018 and 2019, we observed high growth rates over short period of times in spring and summer (Fig. 7). In addition, there was high spatial heterogeneity across the bay, with high positive μ_{NDVI} values observed mainly in the northern and north-western intertidal flats, while growth rates at the south of the bay were very low (Fig. 6). MPB biomass loss rates (negative μ_{NDVI}) were also higher in the north-northwest tidal flats but with an apparent lower interannual variability than for the growing periods.

Net growth and loss rates of MPB biomass varied along the SL intertidal range (Fig. 7). The highest μ_{NDVI} positive and negatives values were observed at the lower intertidal (<-0.75 m) (Fig. 7a, c). Along the intertidal area, mean positive μ_{NDVI} values increased very slightly from the high SL range down to about −0.25 m, increasing more steeply seaward after that SL (Fig. 7c). Interestingly, a similar trend was observed for the mean loss rate of MPB biomass, calculated for non-growing periods. There were differences between years, MPB growth rates showed a more complex pattern in 2018 and 2019, where we recorded high positive values in spring and early summer and negatives values in autumn an early winter (2018) that were nor observed in previous years. Nonetheless these very high positive and negative growth rates phases were mainly observed below a SL of −0.75 m, affecting a very small percentage of the intertidal area (Fig. 7b). This higher variability in the timing of growing periods along the tidal gradient in 2018–2019 coincided with the higher variability in the seasonal trend observed in the mean MPB standing stocks in the same years (Fig. 4b).

4. Discussion

4.1. Mapping intertidal primary producers using a random forest classification algorithm

The present study is the first one in which a random forest (RF) machine learning classification method has been used to analyse the spatial patterns of several communities of primary producers along an intertidal zone during 4 consecutive years. These data further allowed us to study changes in biomass, cover and net growth rate of MPB along the intertidal gradient. Previously, classification methods have been applied to SPOT-6/7 satellite images to study benthic microalgae in the subtidal (St-Pierre and Gagnon, 2020) or to distinguish between seagrass and benthic algae in several bays in Canada (Wilson et al., 2019). Unsupervised and supervised classification methods were applied successfully on IKONOS satellite images (pay-for) to map *Zostera marina* spatial patterns (Pu and Bell, 2017). Recently, Zoffoli et al. (2020) created an algorithm to determine seagrass percent cover in Sentinel-2 images. NDVI was measured radiometrically *in-situ*, in cores which were nadir-viewing photographed, and then *Zostera* sp. percent cover computed using image analysis software. In comparison with these methods, RF machine learning classification allowed us to successfully separate MPB patches, *Zostera sp.*, *Caulerpa* sp. and green macroalgae at the same time. RF has previously been used to map other seagrass species (*Posidonia oceanica* and *Cymodocea nodosa*) using the RapidEye time series (Traganos and Reinartz, 2018). However, in these previous works,

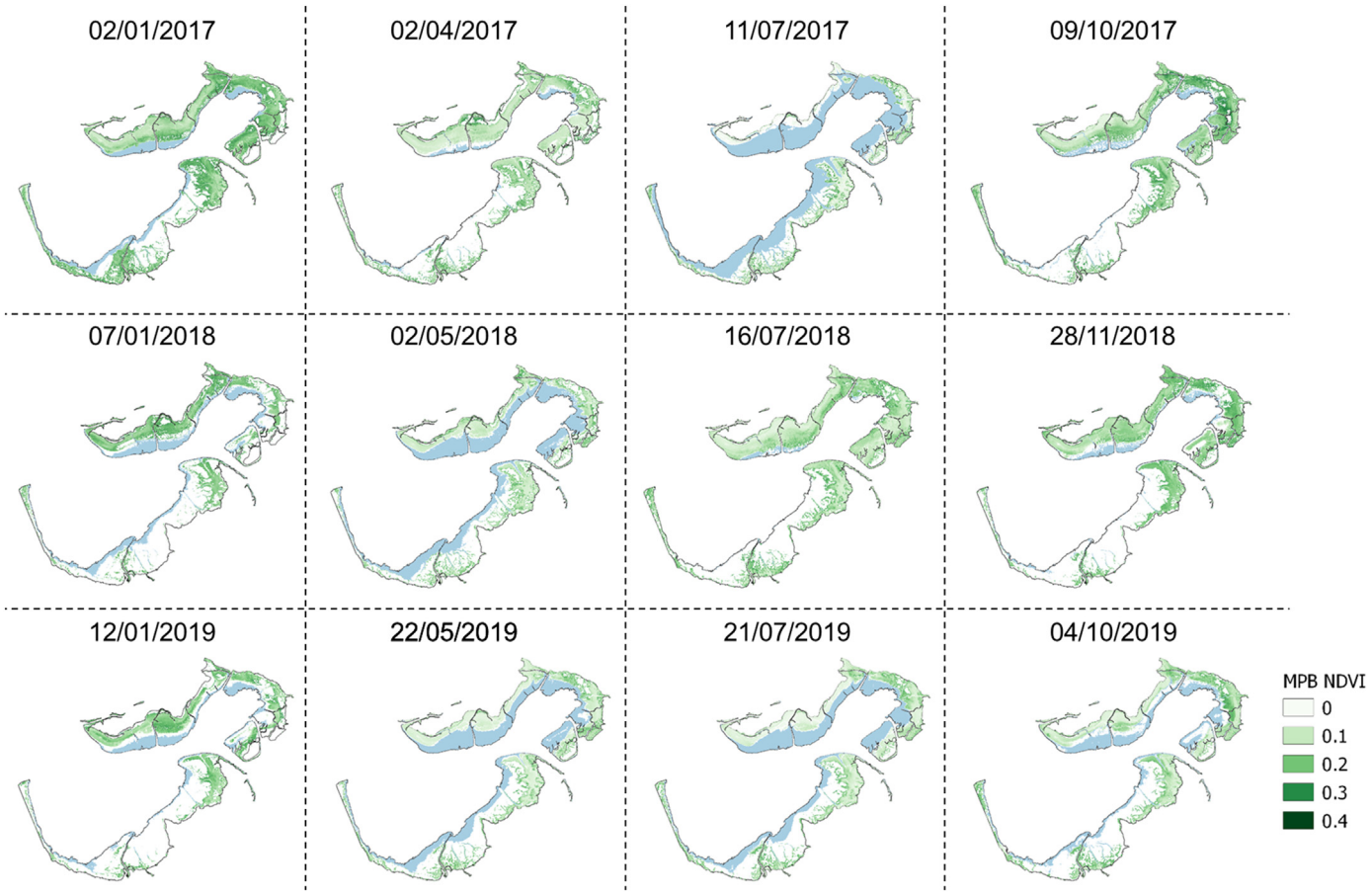

Fig. 3. Maps indicating in the variations of MPB biomass in the intertidal zone of inner Cadiz Bay. Representative images of the four seasons (winter, spring, summer and autumn from left to right) are shown for three consecutive years (2017–2019). MPB was identified by a Normalized Difference Vegetation Index (NDVI) for pixels classified as MPB using Random Forest algorithm from Sentinel-2 images and ranged between 0 and 0.4. Blue colour represents the water cover.

after applying RF no attempt was made to calculate vegetation indexes to estimate biomass pixel^{-1}. To date, only Oiry and Barillé (2021) have used RF to classified MPB (producer's accuracy = 84%) in Sentinel-2 images. Their aim was to develop microphytobenthos-based water quality indices in estuaries and the spatio-temporal patterns of MPB biomass were not analysed.

In our study, the RF algorithm successfully identified the distribution of MPB patches (user's accuracy = 100%), meadows of *Zostera* sp. and *Caulerpa sp.*, as well as of other green macroalgae (*Ulva sp.)* in the intertidal flats of the inner Cadiz Bay (user's accuracy >72% for all categories) (Table 1, Fig. 2). Mean MPB NDVI calculated from Sentinel-2 images ranged between 0 and 0.45 (Supplementary Table 3). This range was slightly higher than the observed by Oiry and Barillé (2021) in 26 coastal systems along the French coast (0 - 0.37) and in other studies where remote sensing was used to analyse spatio-temporal variability of MPB biomass. For example, MPB NDVI range was from 0 to 0.20 in Dutch and English estuaries (Daggers et al., 2018; Van der Wal et al., 2010) and up to 0.35 in French and Portuguese estuaries (Benyoucef et al., 2014; Brito et al., 2013; Echappé et al., 2018; Savelli et al., 2018); however, these studies used different satellite data such as SPOT (Benyoucef et al., 2014; Brito et al., 2013), Landsat (Daggers et al., 2018; Echappé et al., 2018) or MODIS (Savelli et al., 2018; Van der Wal et al., 2010). To date, only Daggers et al. (2020) have used Sentinel-2 images to study seasonal and spatial variability of MPB on extensive bare intertidal flats along the estuarine gradient in the Dutch part of the Westerschelde Estuary. In their study, MPB NDVI oscillated from 0 to 0.27, a range equal to that established previously in the same study site (Daggers et al., 2018). Overall, these ranges were lower than those obtained by measuring at single points on the sediment surface using hand-held spectrometers, where NDVI values of up to 0.65 have been measured for MPB in bare sediment (Barillé et al., 2011; Kromkamp et al., 2020; Serôdio et al., 2009).

Different approaches have been used to distinguish MPB from other benthic communities in remote sensing studies so far. MPB was identified based exclusively on the NDVI range, which was established by a correlation between either MPB Chl-*a* or NDVI calculated from spectral reflectance analysis measured *in situ*, *versus* the NDVI obtained from satellite images (Brito et al., 2013; Daggers et al., 2018; Méléder et al., 2003). Based on these correlations, NDVI values higher than 0.3 were considered macrophytes instead of high MPB biomass (Benyoucef et al., 2014). In a further step to distinguish MPB from other communities, Van der Wal et al. (2010) used vegetation maps and aerial photographs to exclude seagrass meadows and perennial saltmarshes. Recently, geometric masks in GIS were applied to exclude macroalgae (Echappé et al., 2018) and saltmarsh vegetation (Daggers et al., 2020). In our study, a total of 111 visual inspections, in the field and aerial photographs, were necessary to train initially the RF algorithm from all Sentinel-2 spectral bands to distinguish MPB from other benthic communities, taking into account more information than just the NDVI range (Table 1). The results showed a significant improvement compared to previous studies in the simultaneous classification of the different primary producers communities. Using RF, pixels classified as *Zostera* sp. showed a range of NDVI values between 0 and 1 (Supplementary Table 2), *i.e.* RF allowed the classification of pixels as

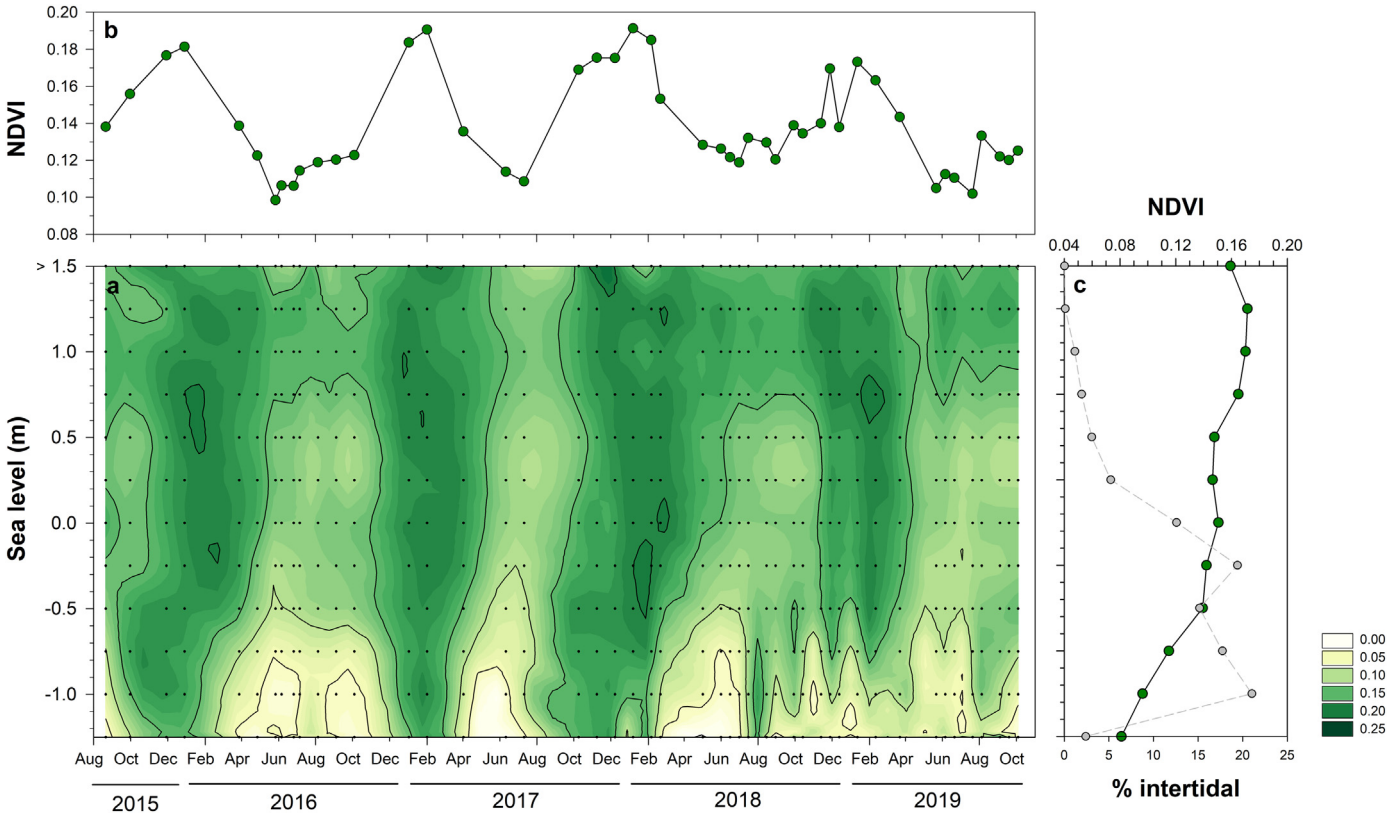

Fig. 4. (a) Contour plot of average MPB biomass, expressed as NDVI pixel^{-1}, per sea level (SL) bin along the intertidal zone of inner Cadiz Bay for each satellite image analysed in the period August 2015 to October 2019. (b) Temporal evolution of average MPB biomass for the entire intertidal zone of inner Cadiz bay. (c) Average MPB biomass along intertidal gradient for each SL bin.

Zostera sp, even when the biomass of *Zostera sp,* was low (<0.4 NDVI) (Barillé et al., 2010). NDVI values for *Caulerpa* sp. were often negative as a consequence of the negative slope in the near infrared of the spectrum reflected by the pixels classified as *Caulerpa sp.* (Supplementary Table 3). This is because meadows of *Caulerpa* sp. were located at the lower fringe of the intertidal SL range, where they were occasionally affected by water reflectance (Fig. 2). To date, the detection of green macroalgae by multispectral remote sensing has been problematic due the difficulty of spectrally discriminating macroalgae from benthic microalgae, with low macroalgal biomass often being confused with high MPB biomass (Van der Wal et al., 2010, 2014). However, using Sentinel-2 combined with RF improved the distinction of MPB from green macroalgae (Oiry and Barillé, 2021). The good performance of RF algorithm in classifying correctly MPB pixels, even in this highly heterogeneous system, was supported by the existence of a significant statistical regression between *in situ* values of MPB Chl-*a* and the corresponding NDVI values obtained from satellite images classified as MPB (Supplementary Fig. 1), as observed in other studies (Brito et al., 2013; Daggers et al., 2018).

Remote sensing in combination with the RF algorithm showed a clear zonation of the vegetation communities on the intertidal zone of the inner Bay of Cadiz, showing at same time a seasonal pattern and some interannual differences in their spatial distribution as well (Fig. 2). MPB coverage dominated the intertidal zone with an average cover of 62%, followed by *Zostera sp.* (30%) and *Caulerpa sp.* (6%). The surface covered by green macroalgae (*Ulva sp.*) was small (2%) and strongly seasonal, being present only in winter as shown previously by field studies (Papaspyrou et al., 2014). Our results clearly show a heterogeneous distribution of these primary producers' communities in inner Cadiz Bay tidal flats, with MPB dominating the intertidal flats located in the north and north-east and *Zostera* sp. and *Caulerpa* sp. mainly concentrated in the south and south-west intertidal flats (Fig. 2). *In situ* observations during years of field studies corroborate this distribution pattern in the intertidal zone (Brun et al., 2015; Haro et al., 2020; Morris et al., 2009). Competition for space between the different intertidal communities is likely to occur. Surface area covered by MPB was inversely and linearly related with surface covered by *Zostera sp.* (Pearson correlation coefficient; $r = -0.84$, $n = 49$, $p < 0.05$) and *Caulerpa sp.* (Pearson correlation coefficient; $r = -0.64$, $n = 49$, $p < 0.005$). However, no significant relationship was observed between the surface covered by MPB and macroalgae or between *Zostera* sp. and *Caulerpa* sp. suggesting an absence of competition for space among these communities. Particularly in the case of *Zostera* sp. and *Caulerpa* sp. the absence of competition could be due to a different preference for an optimal SL range (Morris, 2006). The community maps obtained using the combination of Sentinel-2 images and the RF classification algorithm depicts the vegetal zonation of the whole intertidal area of inner Cadiz Bay with an unprecedented spatial resolution. As shown for MPB in the following sections, this approach can be very useful to analyse the changes in space and time of the main communities of primary producers in this protected shallow environment, not only from the point of view of science but also for their monitoring for conservation and management purposes.

4.2. Spatio-temporal patterns in the MPB biomass and cover

Microphytobenthos presented a consistent and clear spatio-temporal pattern, although some interannual differences in the intensity of MPB NDVI (MPB biomass) and its spatial pattern were also observed from 2017 to 2019 (Figs. 3, 4). The seasonal dynamic of the spatially averaged MPB biomass showed the existence of a clear seasonal maximum in winter and a minimum in summer although not

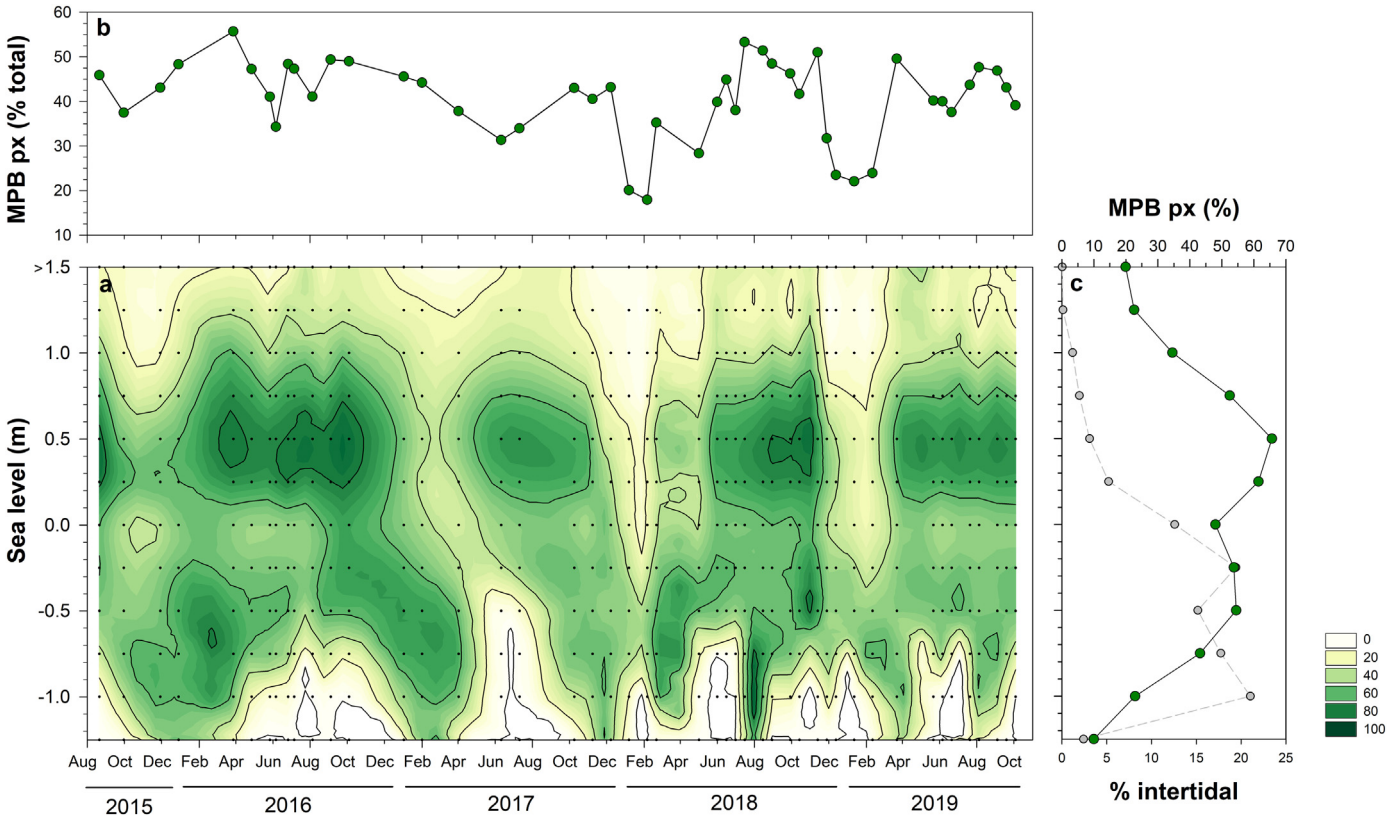

Fig. 5. (a) Contour plot of average spatial cover of MPB biomass, expressed in % of pixels classified as MPB by the Random Forest logarithm, per sea level (SL) bin along the intertidal zone of inner Cadiz Bay for each satellite image analysed in the period August 2015 to October 2019. (b) Cover of MPB biomass along intertidal gradient of mean sea level (m) in the time. (c) Average cover of MPB biomass along intertidal gradient for SL intervals.

necessarily with the same intensity nor at exactly the same days every year (Fig. 4a, Supplementary Fig. 3). This seasonal pattern coincides with previous results obtained by field studies in the inner Cadiz Bay (Garcia-Robledo et al., 2016; Haro et al., 2020; Papaspyrou et al., 2014). However, in northern European estuaries and tidal flats (*e.g.* northern France, United Kingdom and Netherlands), characterised

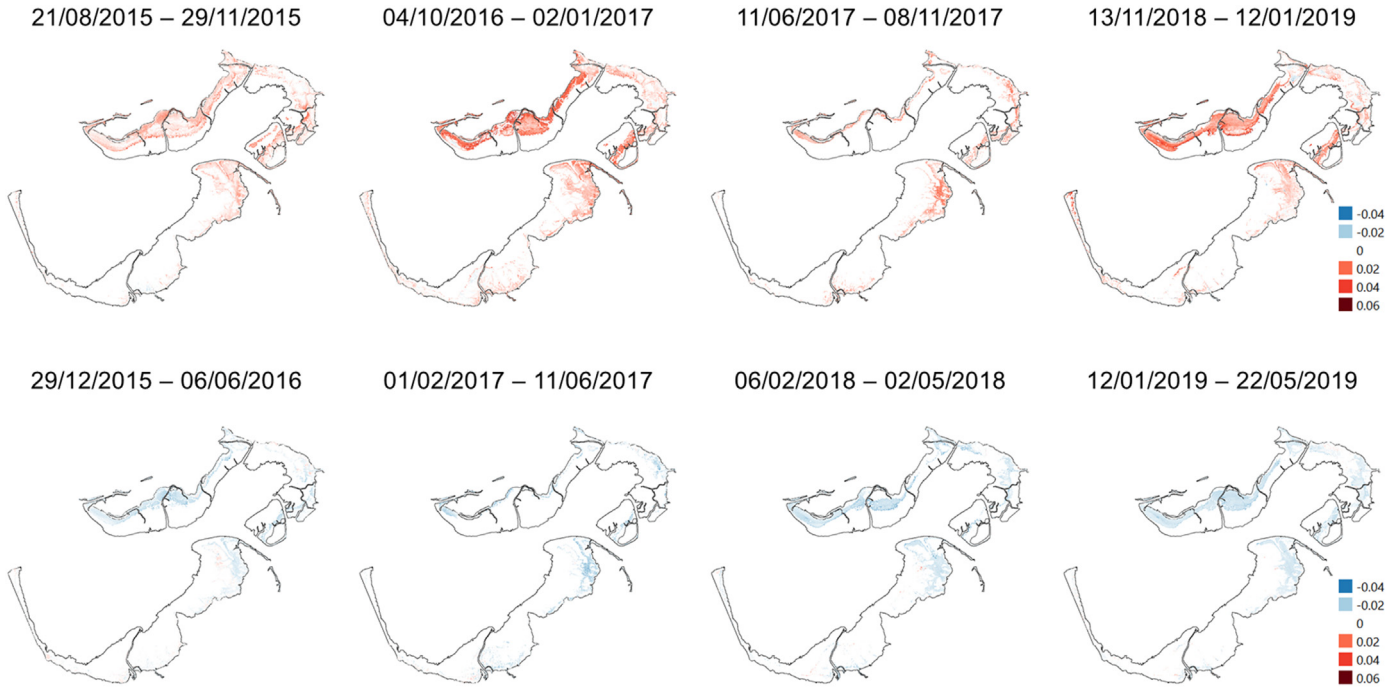

Fig. 6. Net growth rates of MPB biomass (μ_{NDVI}, day^{-1}), estimated from changes in NDVI between satelite images in inner Cadiz bay between minimums and maximums in each year (Fig. 4). Red colour indicates net growth (positive μ_{NDVI}), whereas blue colour indicates net loss in biomass (negative μ_{NDVI}).

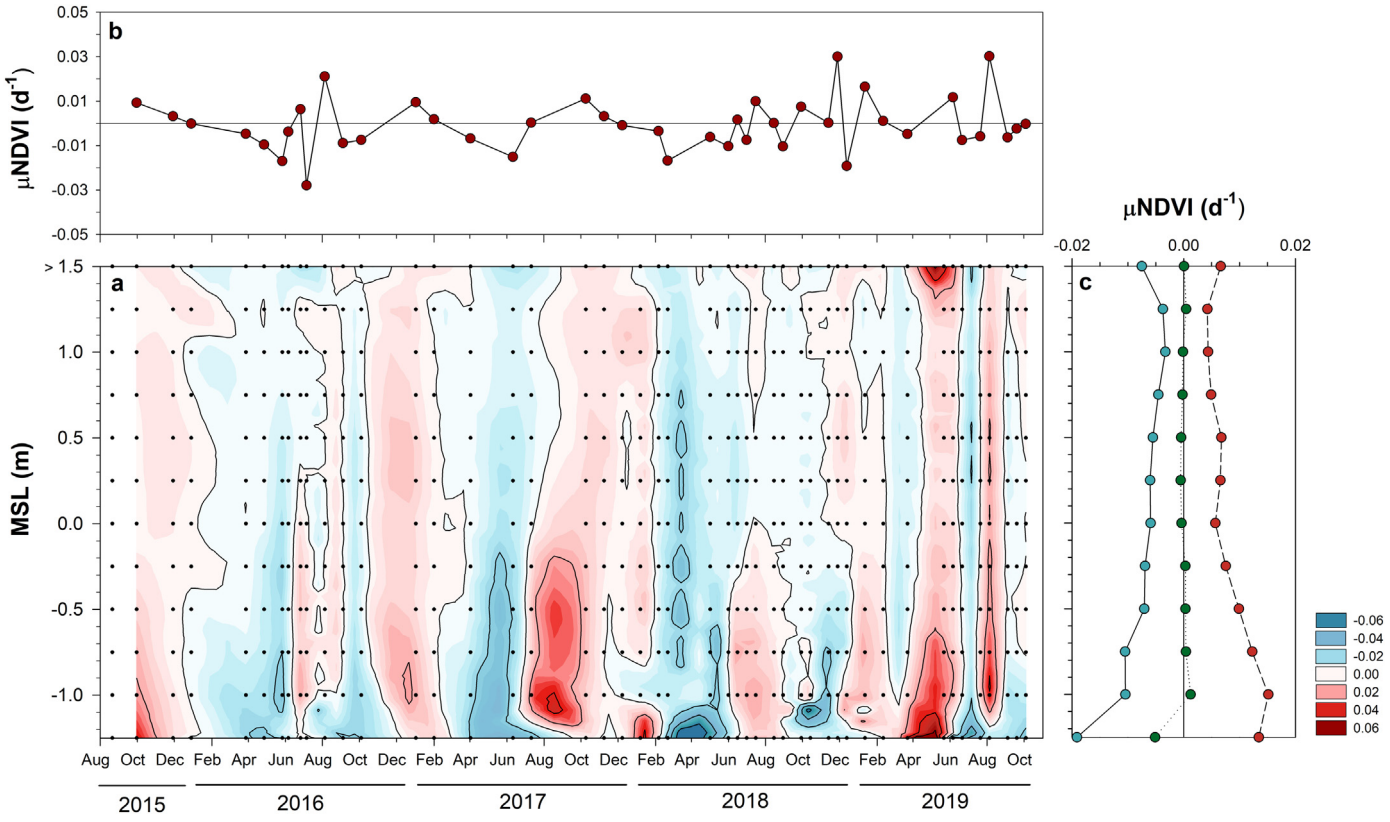

Fig. 7. (a) Contour plot of mean net growth rates of MPB biomass, estimated from changes in NDVI (μ_{NDVI}, day^{-1}), per sea level (SL) along the intertidal zone of inner Cadiz bay for each satellite image analysed in the period August 2015 to October 2019. Negative rates (biomass loss rate) are depicted in different intensities of blue colour, whereas positives rates, corresponding to net increases in the MPB biomass, are represented in different intensities of red. (b) Average μ_{NDVI} along the intertidal gradient of sea level with respect to time. (c) Averaged positive μ_{NDVI} values (red), averaged negative μ_{NDVI} values (blue) and entire data set (positive and negative, green) μ_{NDVI} values values over time with respect to SL.

by temperate humid climate with typically cold winters and mild summers, the annual MPB biomass maximum tends to occur in spring or summer (Benyoucef et al., 2014; Ubertini et al., 2012; Van der Wal et al., 2010). A seasonal MPB biomass winter maximum, like the one observed in our study has been observed in other coastal areas and estuaries with warm temperate climate with mild winters and hot summers; for example, in Europe, the Tagus estuary in Portugal (Brito et al., 2013), the Brouage mud flat in the Atlantic coast of France (Savelli et al., 2018); and in Asia, the Ariake Sea in Japan (Koh et al., 2007), the upper intertidal shore of Changjiang (Yangtze) estuary in central China (Zhang et al., 2021) and several mud flats in west Korea (Kwon et al., 2018, 2016). Climatic conditions control environmental variables such as irradiance and temperature which could be directly or indirectly responsible for the seasonal MPB patterns observed in intertidal flats around the world (Kwon et al., 2020). The high irradiance and temperatures recorded at midday during summer in the south of Europe and other temperate areas could inhibit the growth of MPB due to photoinhibition, desiccation, or an increase in interstitial water salinity (Coelho et al., 2009; Savelli et al., 2018; Underwood et al., 1998). Recently, Zhang et al. (2021) determined that the distribution of MPB biomass along the intertidal gradient depended on season. In Cadiz Bay, an inverse correlation between MPB biomass and air temperature was observed, indicating that summer conditions are not optimal for MPB standing stocks (Supplementary Fig. 2). In addition to air temperature, mean wind speed seems to have a statistically significant negative effect on MPB biomass standing stocks, likely due to the MPB resuspension and higher turbidity in the water column as a consequence of wind induced turbulence during high tide (Ubertini et al., 2012) and sediment desiccation during low tide. An additional top down control by grazing, which is usually higher in summer, could also play a role for the seasonal patterns observed in the Cadiz Bay (Coelho et al., 2011; Haro et al., 2020; Savelli et al., 2018; Ubertini et al., 2012). However, grazing by benthic fauna seems to affect spatial variability of MPB at micro-scale (up to about 1 m) but not at meso- and macro-scale, where bottom-up mechanisms seem to be more relevant (Daggers et al., 2020; Weerman et al., 2011).

Despite the seasonal and interannual variability in the intensity MPB NDVI and in the size and spatial distribution of the MPB patches, a clear MPB biomass spatial patterns was recorded both across the entire bay's intertidal zone (Fig. 3) and along the intertidal SL gradient (Fig. 4). The distribution of MPB biomass in the intertidal zone across the bay was not homogeneous, with higher levels of MPB biomass per pixel and higher surface area covered observed mainly in the tidal zones located in the north and north-west of the bay in all seasons. Contrastingly, lower MPB biomass and cover were observed in the south-western tidal flats. Differences in the sediment mean grain size, sediment elevation and hydrodynamic conditions between these zones can explain the colonization extent and biomass levels of MPB in Cadiz Bay, as reported elsewhere (Benyoucef et al., 2014; Brito et al., 2013; Guarini et al., 1998; Orvain et al., 2012; Van der Wal et al., 2010). The sediment in the north and north-east of inner Cadiz is muddier, favouring MPB growth (Orvain et al., 2012), whereas it is sandier in the south and south-west (Freitas et al., 2008; Haro et al., 2020; Sanchez De Lamadrid Rey and Muñoz Pérez, 1994). However, Haro et al. (2020) showed that seasonal changes in MPB biomass, estimated by Chl-*a*, and MPB net primary production along two intertidal transects with different SL in the inner Cadiz Bay (red dots in Fig. 1) could not be associated to a single ecological variable. Furthermore, the set of ecological variables contributing more to explain the seasonal and spatial changes in MPB biomass or net primary production differed between transects, one located in the northeastern

(muddier) and the other in the southern part (sandier) of inner Cadiz Bay. Meteorological variables (irradiance and temperature), SL, grain size, organic carbon and total nitrogen content in the sediment and water column and porewater nutrients contributed in different degrees to explain the spatio-temporal changes in MPB Chl-*a* and P_N. Recently, Daggers et al. (2020) showed that MPB patchiness and patch size differed between different intertidal ecotopes in the Westerschelde Estuary. The geomorphological and hydrodynamic characteristics of ecotopes are known to determine many other ecological variables, like immersion and emersion periods, daily irradiance dose, resuspension rates, organic matter content, porewater nutrients, *etc.*, which directly affect benthic communities (Baptist et al., 2019; Bouma et al., 2005). Ecotopes have not been explicitly identified in the inner Cadiz Bay so far, but clear differences in grain size distribution, hydrodynamics and the slope and extension of the intertidal flats exist between the north-northeast and the south-southwest regions of the bay (Freitas et al., 2008; Haro et al., 2020; Sanchez De Lamadrid Rey and Muñoz Pérez, 1994).

The spatio-temporal pattern of MPB biomass and MPB cover in relation to SL of the intertidal areas of the inner Cadiz Bay was different. While MPB biomass decreased significantly with SL, MPB cover presented a bimodal distribution, showing a large peak at about +0.5 m and a secondary peak at −0.5 m SL (Fig. 4a, c; Fig. 5a, c). Additionally, temporal changes in mean MPB biomass and MPB cover were not significantly correlated (Fig. 4b, Fig. 5b). The general trend of MPB biomass decreasing seaward has been observed in other ecosystems, being attributed to the lower amount of light received at the lower shore due to reduced exposure time during emersion and larger water columns during immersion (Brito et al., 2013; Jesus et al., 2009; Kwon et al., 2016; Orvain et al., 2012; Van der Wal et al., 2010). However, in other ecosystems MPB biomass along the tidal range followed a bimodal distribution, with MPB biomass peaks in the middle and upper shore (Benyoucef et al., 2014; Davoult et al., 2009). Lower values of MPB biomass in the upper fringe in summer and at the beginning of autumn with respect to winter has been reported as well and attributed to the higher temperatures reached at the sediment surface, and thus higher sediment desiccation in warmer seasons (Brito et al., 2013; Savelli et al., 2018). This suggests a rather complex ecological regulation of the MPB spatio-temporal dynamics, where biotic and abiotic factors likely interact, resulting, on occasion, in bimodal distributions of MPB biomass and/or cover along the intertidal gradient (Underwood, 2001). The lack of covariance between the general distribution of MPB biomass and MPB cover (Figs. 4, 5), suggests differences in their ecological regulation. The relationship between MPB biomass density and cover are likely complex and could be site-dependent. Guarini et al. (1998) proposed the "constant-density model" for Marennes-Oleron Bay (France), in which MPB biomass density within a given patch remains constant and the patch size increases during the growing season and therefore percentage of cover. Contrastingly, Daggers et al. (2020) proposed a "proportional-density model" for MPB dynamics in Westerschelde Estuary (The Netherlands), where the patch size remains constant and the biomass density increases within the patch. Nonetheless, both authors pointed out that local, site-specific environmental conditions might determine pattern formation and the relationship between MPB biomass and patchiness. Given the variation between proposed models for different ecosystems, further research is needed to test their degree of universality and identify the ecological factors involved in the differences in the patterns of MPB biomass, cover and patchiness. Remote sensing tools such as the ones used here are of great importance, being able to cover large spatial scales over long periods of time.

4.3. Growth rates of MPB biomass

Net growth rates of MPB biomass (μ_{NDVI}) showed considerable temporal (seasonal pattern and interannual variability) and spatial heterogeneity (along the SL range and between different tidal flats in the inner bay) (Fig. 6). Most μ_{NDVI} values in the tidal flats of Cadiz Bay (~96% within $\pm 0.06\ d^{-1}$) were in the same order of magnitude than the values reported in the few published studies where MPB growth rate has been determined *in situ* (0.1 d^{-1}, Admiraal and Peletier, 1980; 0.06–0.27 d^{-1}, Gould and Gallagher, 1990; 0.02 d^{-1}, Kromkamp et al., 2020). Typically, MPB growth rates measured in laboratory cultures are higher than *in situ* net rates due to optimised growth conditions and the elimination of competition and grazing (0.18–1.5 d^{-1}, Admiraal et al., 1982; Hillebrand and Sommer, 1999; Scholz and Liebezeit, 2012; Underwood and Smith, 1998).

The spatial distribution of μ_{NDVI} presented clear interannual differences in the timing, extension and intensity of net growth rates (Figs. 6, 7). Maximum positive μ_{NDVI} were generally observed at the intertidal flats located in the northern area of the bay, while little or no changes were detected in most of the intertidal zones located in the southern part (Fig. 6). This confirms that the former seems to be better suited for MPB growth, likely due to lower sediment particle size and other ecotopes' characteristics compared to the latter, which is sandier and with a higher covers of *Zostera* sp. *and Caulerpa sp.* (Fig. 2). However, since the vertical distribution of MPB biomass is more homogeneous, reaching deeper in sandy sediment respect to muddy sediment, remote sensing techniques might underestimate the total areal standing stocks of MPB biomass in sandy sediment affecting as well the estimation of net growth rate by remote sensing as performed here (Jesus et al., 2006). MPB biomass and net growth rate are under the control of a high number of biotic and abiotic ecological factors, *e.g.* temperature, irradiance, salinity, sediment grain size, nutrients, grazing, *etc.* (Admiraal et al., 1982; Hillebrand and Sommer, 1999; Orvain et al., 2012; Scholz and Liebezeit, 2012; Underwood and Provot, 2000; Weerman et al., 2011), whose importance probably changes seasonally and spatially at micro- and mesoscale (Daggers et al., 2020; Van der Wal et al., 2010; Weerman et al., 2011). To a large extent, the wide environmental variability that intertidal MPB communities experience is related directly or indirectly to their position along the tidal SL range, which most likely affects the standing stocks of MPB biomass, cover and the mean net growth rates. The position of the MPB community in the SL tidal range determines the daily emersion/immersion times and the daily irradiance dose, which is an essential variable to model standing stocks of MPB biomass and primary production of intertidal MPB (Pinckney and Zingmark, 1991, Serôdio and Catarino, 2000, Savelli et al., 2018, Daggers et al., 2018). In contrast to the general trend of MPB biomass and cover decreasing seaward along the intertidal SL range in the inner Cadiz Bay, we observed higher positive net growth rates (positive μ_{NDVI}) at lower SL. It is interesting to note that net biomass loss rate (negative μ_{NDVI}) was also higher at lower SL. We are not aware of any other study analysing spatio-temporal changes in MPB growth rate with the spatial range and resolution done here (Daggers et al., 2020; Méléder et al., 2020; Savelli et al., 2020). So far, it is unclear whether the pattern in the μ_{NDVI} spatial changes observed in the inner Cadiz Bay occur in similar intertidal ecosystems in other geographical regions. In temperate low latitude intertidal zones, a low position in the SL range would assure less variable growing conditions, with shorter emersion periods, smaller temperature shift range and higher access to water column nutrients, all favouring higher growth rates (Bohórquez et al., 2019; Garcia-Robledo et al., 2016). Simultaneously, the higher loss rates of MPB biomass at lower SL might also be a consequence of higher grazing and bioturbation rates or stronger resuspension events (Ubertini et al., 2012). Additionally, it is likely that the relative weight of the different ecological drivers, biotic and abiotic, affecting the MPB community (taxonomic composition, biomass, cover, growth rate) change along the SL gradient.

5. Conclusion

Remote sensing is a powerful tool, with free and open-source Sentinel imagery providing a great opportunity for monitoring intertidal communities of primary producers due to its enhanced spatial, spectral and temporal resolution. These properties allow an

unprecedented analysis of the spatio-temporal dynamics of biomass, cover and net growth rate of benthic communities at different spatial scales. By applying a Random Forest algorithm machine learning classification method, we were able to successfully distinguish and map different intertidal primary producers' communities. Here we have focused on the analysis of the changes in MPB biomass and cover along the intertidal range over a period of 4 years. The results allowed us to present, for the first time as far as we know, the spatio-temporal changes of the MPB biomass and cover patterns in high resolution and testing previously suggested seasonal and SL gradient patterns and models. Additionally, we were able to estimate MPB growth and loss rates for the entire intertidal area of the Cadiz Bay in relation to SL, at the same high spatio-temporal resolution. The observed differences in the patterns of the MPB community features explored here, *i.e.* biomass, cover and net growth and loss rate, open interesting new research questions related to their universality in different coastal ecosystems and across latitude, and on what are the ecological drivers responsible for them. High resolution remote sensing in combination with machine learning algorithms allows the systematic investigation of these features in MPB and other benthic communities, taking into account the spatial heterogeneity of the intertidal environment at different scales. Thus, producing a more integral view of this important interface between the terrestrial and the marine environments in shallow coastal areas.

Funding

This project was funded by the Spanish Ministry of Economy and Business (MINECO) through the project MICROBAHIA2 (CTM2017-82274-R) awarded to AC, and EXTREME-FUN (PID2020-112488RB-I00) awarded to SP and AC. SH was funded by a postdoctoral fellowship from the University of Cádiz, Spain (2018-011/PU/AY.PUENTE/CD; 2019-004/PU/PP-EST/MV).

CRediT authorship contribution statement

S. Haro: Conceptualization, Software, Investigation, Writing – original draft, Visualization. **B. Jesus:** Conceptualization, Software, Writing – review & editing, Supervision. **S. Oiry:** Methodology. **S. Papaspyrou:** Conceptualization, Formal analysis, Writing – review & editing, Visualization. **M. Lara:** Conceptualization, Formal analysis, Writing – original draft. **C.J. González:** Visualization. **A. Corzo:** Conceptualization, Writing – original draft, Writing – review & editing, Visualization, Funding acquisition.

Declaration of competing interest

The authors declare that they have no known competing financial interests or personal relationships that could have appeared to influence the work reported in this paper.

Acknowledgments

This research is the result of a collaboration between the Remote Sensing and Benthic Ecology Group (University of Nantes, France) and The Microbial Ecology and Biogeochemistry Laboratory (University of Cadiz, Spain).

Appendix A. Supplementary data

Supplementary data to this article can be found online at https://doi.org/10.1016/j.scitotenv.2021.149983.

References

Admiraal, W., Peletier, H., 1980. Influence of seasonal variations of temperature and light on the growth rate of cultures and natural populations of intertidal diatoms. Mar. Ecol. Prog. Ser. 2, 35–43. https://doi.org/10.3354/meps002035.

Admiraal, W., Peletier, H., Zomer, H., 1982. Observations and experiments on the population dynamics of epipelic diatoms from an estuarine mudflat. Estuar. Coast. Shelf Sci. 14, 471–487. https://doi.org/10.1016/S0302-3524(82)80071-6.

Asmus, H., Asmus, R., 2000. Material exchange and food web of seagrass beds in the sylt-Rømø bight: how significant are community changes at the ecosystem level? Helgol. Mar. Res. 54, 137–150. https://doi.org/10.1007/s101520050012.

Baptist, M.J., van der Wal, J.T., Folmer, E.O., Gräwe, U., Elschot, K., 2019. An ecotope map of the trilateral Wadden Sea. J. Sea Res. 152, 101761. https://doi.org/10.1016/j.seares.2019.05.003.

Barillé, L., Robin, M., Harin, N., Bargain, A., Launeau, P., 2010. Increase in seagrass distribution at Bourgneuf Bay (France) detected by spatial remote sensing. Aquat. Bot. 92, 185–194. https://doi.org/10.1016/j.aquabot.2009.11.006.

Barillé, L., Mouget, J.-L., Méléder, V., Rosa, P., Jesus, B., 2011. Spectral response of benthic diatoms with different sediment backgrounds. Remote Sens. Environ. 115, 1034–1042. https://doi.org/10.1016/j.rse.2010.12.008.

Barinova, S., Bondarenko, A., Ryabushko, L., Kapranov, S., 2019. Microphytobenthos as an indicator of water quality and organic pollution in the western coastal zone of the sea of Azov. Oceanol. Hydrobiol. Stud. 48, 125–139. https://doi.org/10.1515/ohs-2019-0013.

Benyoucef, I., Blandin, E., Lerouxel, A., Jesus, B., Rosa, P., Méléder, V., Launeau, P., Barillé, L., 2014. Microphytobenthos interannual variations in a north-european estuary (Loire estuary, France) detected by visible-infrared multispectral remote sensing. Estuar. Coast. Shelf Sci. 136, 43–52. https://doi.org/10.1016/j.ecss.2013.11.007.

Bishop-Taylor, R., Sagar, S., Lymburner, L., Beaman, R.J., 2019. Between the tides: modelling the elevation of Australia's exposed intertidal zone at continental scale. Estuar. Coast. Shelf Sci. 223, 115–128. https://doi.org/10.1016/j.ecss.2019.03.006.

Bohórquez, J., McGenity, T.J., Papaspyrou, S., Garcia-Robledo, E., Corzo, A., Underwood, G.J.C., 2017. Different types of diatom-derived extracellular polymeric substances drive changes in heterotrophic bacterial communities from intertidal sediments. Front. Microbiol. 8, 245. https://doi.org/10.3389/fmicb.2017.00245.

Bohórquez, J., Calenti, D., Garcia-Robledo, E., Papaspyrou, S., Jimenez-Arias, J.L., Gómez-Ramírez, E.H., Corzo, A., 2019. Water column dissolved silica concentration limits microphytobenthic primary production in intertidal sediments. J. Phycol. 55, 625–636. https://doi.org/10.1111/jpy.12838.

Bouma, H., de Jong, D.J., Twisk, F., Wolfstein, K., 2005. A Dutch Ecotope System for Coastal Waters (ZES.1). Middelburg, Rep. RIKZ/2005.024 English Version June 2006.

Breiman, L., 2001. Random forests. Mach. Learn. 45, 5–32. https://doi.org/10.1023/A:1010933404324.

Brito, A.C., Benyoucef, I., Jesus, B., Brotas, V., Gernez, P., Mendes, C.R., Launeau, P., Dias, M.P., Barillé, L., 2013. Seasonality of microphytobenthos revealed by remote-sensing in a south european estuary. Cont. Shelf Res. 66, 83–91. https://doi.org/10.1016/j.csr.2013.07.004.

Brun, F.G., Vergara, J.J., Morris, E.P., 2015. Diversidad de angiospermas marinas en la bahía de Cádiz : redescubriendo a Zostera marina. Chron. Naturae 5, 45–56.

Canfield, D.E., Thamdrup, B., Kristensen, E., 2005. Aquatic Geomicrobiology. Advances in Marine Biology. Elsevier Academic Press.

Casal, G., Sánchez-Carnero, N., Sánchez-Rodríguez, E., Freire, J., 2011. Remote sensing with SPOT-4 for mapping kelp forests in turbid waters on the south european Atlantic shelf. Estuar. Coast. Shelf Sci. 91, 371–378. https://doi.org/10.1016/j.ecss.2010.10.024.

Coelho, H., Vieira, S., Serôdio, J., 2009. Effects of desiccation on the photosynthetic activity of intertidal microphytobenthos biofilms as studied by optical methods. J. Exp. Mar. Bio. Ecol. 381, 98–104. https://doi.org/10.1016/j.jembe.2009.09.013.

Coelho, H., Cartaxana, P., Brotas, V., Queiroga, H., Serôdio, J., 2011. Pheophorbide a in Hydrobia ulvae faecal pellets as a measure of microphytobenthos ingestion: variation over season and period of day. Aquat. Biol. 13, 119–126. https://doi.org/10.3354/ab00356.

Congalton, R.G., 1991. A review of assessing the accuracy of classifications of remotely sensed data. Remote Sens. Environ. 37, 35–46. https://doi.org/10.1016/0034-4257(91)90048-B.

Daggers, T.D., Kromkamp, J.C., Herman, P.M.J., van der Wal, D., 2018. A model to assess microphytobenthic primary production in tidal systems using satellite remote sensing. Remote Sens. Environ. 211, 129–145. https://doi.org/10.1016/j.rse.2018.03.037.

Daggers, T.D., Herman, P.M.J., van der Wal, D., 2020. Seasonal and spatial variability in patchiness of microphytobenthos on intertidal flats from Sentinel-2 satellite imagery. Front. Mar. Sci. 7, 1–14. https://doi.org/10.3389/fmars.2020.00392.

Daughtry, C.S.T., Walthall, C.L., Kim, M.S., Brown de Colstoun, E., McMurtrey III, J.E., 2000. Estimating corn leaf chlorophyll concentration from leaf and canopy reflectance. Remote Sens. Environ. 74, 229–239. https://doi.org/10.3184/174751911X556684.

Davoult, D., Migné, A., Créach, A., Gévaert, F., Hubas, C., Spilmont, N., Boucher, G., 2009. Spatio-temporal variability of intertidal benthic primary production and respiration in the western part of the Mont Saint-Michel Bay (Western English Channel, France). Hydrobiologia 620, 163–172. https://doi.org/10.1007/s10750-008-9626-3.

Day, J.W., Yáñez-Arancibia, A., Kemp, W.M., Crump, B.C., 1990. Estuarine ecology. Estuaries 13, 112. https://doi.org/10.2307/1351438.

Echappé, C., Gernez, P., Méléder, V., Jesus, B., Cognie, B., Decottignies, P., Sabbe, K., Barillé, L., 2018. Satellite remote sensing reveals a positive impact of living oyster reefs on microalgal biofilm development. Biogeosciences 15, 905–918. https://doi.org/10.5194/bg-15-905-2018.

Egea, L.G., Jiménez-Ramos, R., Hernández, I., Brun, F.G., 2019. Effect of in situ short–term temperature increase on carbon metabolism and dissolved organic carbon (DOC)

fluxes in a community dominated by the seagrass Cymodocea nodosa. PLoS One 14, e0210386. https://doi.org/10.1371/journal.pone.0210386.
Frankenbach, S., Ezequiel, J., Plecha, S., Goessling, J.W., Vaz, L., Kühl, M., Dias, J.M., Vaz, N., Serôdio, J., 2020. Synoptic spatio-temporal variability of the photosynthetic productivity of microphytobenthos and phytoplankton in a tidal estuary. Front. Mar. Sci. 7. https://doi.org/10.3389/fmars.2020.00170.
Freitas, R., Rodrigues, A.M., Morris, E.P., Perez-Llorens, J.L., Quintino, V., 2008. Single-beam acoustic ground discrimination of shallow water habitats: 50 kHz or 200 kHz frequency survey? Estuar. Coast. Shelf Sci. 78, 613–622. https://doi.org/10.1016/j.ecss.2008.02.007.
Garcia-Robledo, E., Corzo, A., Papaspyrou, S., Morris, E.P., 2012. Photosynthetic activity and community shifts of microphytobenthos covered by green macroalgae. Environ. Microbiol. Rep. 4, 316–325. https://doi.org/10.1111/j.1758-2229.2012.00335.x.
Garcia-Robledo, E., Bohórquez, J., Corzo, A., Jimenez-Arias, J.L., Papaspyrou, S., 2016. Dynamics of inorganic nutrients in intertidal sediments: porewater, exchangeable, and intracellular pools. Front. Microbiol. 7, 761. https://doi.org/10.3389/fmicb.2016.00761.
Gómez Ordoñez, E., 2008. Propiedades ópticas y teledetección de macrófitos marinos en la bahía de Cádiz. España. Biol. Dep. Univ, Cádiz, p. 23.
Gould, D.M., Gallagher, E.D., 1990. Field measurement of specific growth rate, biomass, and primary production of benthic diatoms of Savin Hill Cove, Boston. Limnol. Oceanogr. 35, 1757–1770. https://doi.org/10.4319/lo.1990.35.8.1757.
Guarini, J.-M., Blanchard, G.F., Bacher, C., Gros, P., Riera, P., Richard, P., Gouleau, D., Galois, R., Prou, J., Sauriau, P.-G., 1998. Dynamics of spatial patterns of microphytobenthic biomass:inferences from a geostatistical analysis of two comprehensive surveys in marennes-Oléron Bay (France). Mar. Ecol. Prog. Ser. 166, 131–141. https://doi.org/10.3354/meps166131.
Haro, S., Bohórquez, J., Lara, M., Garcia-Robledo, E., González, C.J., Crespo, J.M., Papaspyrou, S., Corzo, A., 2019. Diel patterns of microphytobenthic primary production in intertidal sediments: the role of photoperiod on the vertical migration circadian rhythm. Sci. Rep. 9, 13376. https://doi.org/10.1038/s41598-019-49971-8.
Haro, S., Lara, M., Laiz, I., González, C.J., Bohórquez, J., Garcia-Robledo, E., Corzo, A., Papaspyrou, S., 2020. Microbenthic net metabolism along intertidal gradients (Cadiz Bay, SW Spain): spatio-temporal patterns and environmental factors. Front. Mar. Sci. 7. https://doi.org/10.3389/fmars.2020.00039.
Hillebrand, H., Sommer, U., 1999. The nutrient stoichiometry of benthic microalgal growth: Redfield proportions are optimal. Limnol. Oceanogr. 44, 440–446. https://doi.org/10.4319/lo.1999.44.2.0440.
Jesus, B., Brotas, V., Marani, M., Paterson, D.M., 2005. Spatial dynamics of microphytobenthos determined by PAM fluorescence. Estuar. Coast. Shelf Sci. 65, 30–42. https://doi.org/10.1016/j.ecss.2005.05.005.
Jesus, B., Mendes, C.R., Brotas, V., Paterson, D.M., 2006. Effect of sediment type on microphytobenthos vertical distribution: modelling the productive biomass and improving ground truth measurements. J. Exp. Mar. Bio. Ecol. 332, 60–74. https://doi.org/10.1016/j.jembe.2005.11.005.
Jesus, B., Brotas, V., Ribeiro, L., Mendes, C.R., Cartaxana, P., Paterson, D.M., 2009. Adaptations of microphytobenthos assemblages to sediment type and tidal position. Cont. Shelf Res. 29, 1624–1634. https://doi.org/10.1016/j.csr.2009.05.006.
Jimenez-Arias, J.L., Morris, E.P., Rubio-de-Inglés, M.J., Peralta, G., Garcia-Robledo, E., Corzo, A., Papaspyrou, S., 2020. Tidal elevation is the key factor modulating burial rates and composition of organic matter in a coastal wetland with multiple habitats. Sci. Total Environ. 724, 138205. https://doi.org/10.1016/j.scitotenv.2020.138205.
Kaufman, Y.J., Tanré, D., 1992. Atmospherically Resistant Vegetation Index (ARVI) for EOS-MODIS. IEEE Trans. Geosci. Remote Sens. https://doi.org/10.1109/36.134076.
Koh, C.H., Khim, J.S., Araki, H., Yamanishi, H., Kenichi, K., 2007. Within-day and seasonal patterns of microphytobenthos biomass determined by co-measurement of sediment and water column chlorophylls in the intertidal mudflat of nanaura. Estuar. Coast. Shelf Sci. 72, 42–52. https://doi.org/10.1016/j.ecss.2006.10.005.
Kromkamp, J.C., Morris, E., Forster, R.M., 2020. Microscale variability in biomass and photosynthetic activity of microphytobenthos during a spring-neap tidal cycle. Front. Mar. Sci. 7, 1–15. https://doi.org/10.3389/fmars.2020.00562.
Kühl, M., Lassen, C., Jørgensen, B.B., 1994. Optical properties of microbial mats: light measurements with fiber-optic microprobes. Microbial Mats. Springer, Berlin Heidelberg, pp. 149–166 https://doi.org/10.1007/978-3-642-78991-5_16.
Kuhn, Max, Weston, Steve, Williams, Andre, Keefer, Chris, Engelhardt, Allan, Cooper, Tony, Mayer, Zachary, Kenkel, Brenton, Benesty, Michael, Lescarbeau, Reynald, Ziem, Andrew, Scrucca, Luca, Tang, Yuan, Candan, Can, Hunt, Tyler, Jed Wing, Contributions from, the R Core Team, 2018. caret: Classification and Regression Training. R package version 6.0-81. https://CRAN.R-project.org/package=caret.
Kwon, B.-O., Lee, Y., Park, J., Ryu, J., Hong, S., Son, S.H., Lee, S.Y., Nam, J., Koh, C.H., Khim, J.S., 2016. Temporal dynamics and spatial heterogeneity of microalgal biomass in recently reclaimed intertidal flats of the Saemangeum area, Korea. J. Sea Res. 116, 1–11. https://doi.org/10.1016/j.seares.2016.08.002.
Kwon, B.-O., Kim, H.C., Koh, C.H., Ryu, J., Son, S.H., Kim, Y.H., Khim, J.S., 2018. Development of temperature-based algorithms for the estimation of microphytobenthic primary production in a tidal flat: a case study in Daebu mudflat, Korea. Environ. Pollut. 241, 115–123. https://doi.org/10.1016/j.envpol.2018.05.032.
Kwon, B., Kim, H., Noh, J., Yip, S., Nam, J., Seong, J., 2020. Spatiotemporal variability in microphytobenthic primary production across bare intertidal flat, saltmarsh, and mangrove forest of Asia and Australia. Mar. Pollut. Bull. 151, 110707. https://doi.org/10.1016/j.marpolbul.2019.110707.
Lara, M., Peralta, G., Morris, E.P., Bouma, T., Pérez-Lloréns, J.L., 2012. Interacción entre las praderas de angiospermas marinas y la hidrodinámica en el Parque Natural Bahía de Cádiz: Implicaciones ecológicas. ISM12.
Lara, M., Bouma, T.J., Peralta, G., Van Soelen, J., Pérez-Lloréns, J.L., 2016. Hydrodynamic effects of macrophyte microtopography: spatial consequences of interspecific benthic transitions. Mar. Ecol. Prog. Ser. 561, 123–136. https://doi.org/10.3354/meps11913.
Lebreton, B., Rivaud, A., Picot, L., Prévost, B., Barillé, L., Sauzeau, T., Beseres Pollack, J., Lavaud, J., 2019. From ecological relevance of the ecosystem services concept to its socio-political use. the case study of intertidal bare mudflats in the marennes-Oléron Bay, France. Ocean Coast. Manag. 172, 41–54. https://doi.org/10.1016/j.ocecoaman.2019.01.024.
Li, J., Gao, S., Wang, Y., 2010. Invading cord grass vegetation changes analyzed from landsat-TM imageries: a case study from the wanggang area, Jiangsu coast, eastern China. Acta Oceanol. Sin. 29, 26–37. https://doi.org/10.1007/s13131-010-0034-y.
Li, W., Du, Z., Ling, F., Zhou, D., Wang, H., Gui, Y., Sun, B., Zhang, X., 2013. A comparison of land surface water mapping using the normalized difference water index from TM, ETM+ and ALI. Remote Sens. 5, 5530–5549. https://doi.org/10.3390/rs5115530.
Luo, Y., Wang Xinhui Liu, T., 2018. Mapping Plant Communities in the Intertidal Zones of the Yellow River Delta Using Sentinel-2 Optical and Sentinel-1 SAR Time Series Data.
MacIntyre, H.L., Geider, R.J., Miller, D.C., 1996. Microphytobenthos: the ecological role of the "Secret garden" of unvegetated, shallow-water marine habitats. I. Distribution, abundance and primary production. Estuaries 19, 186. https://doi.org/10.2307/1352224.
Mansfield, T.A., Sanith, P.J., 1984. Circadian rhythms. In: Wilkins, M.B. (Ed.), Advanced Plant Physiology. Pitman Publishing Limited, pp. 201–216.
McFeeters, S.K., 1996. The use of the normalized difference water index (NDWI) in the delineation of open water features. Int. J. Remote Sens. 17, 1425–1432. https://doi.org/10.1080/01431169608948714.
Méléder, V., Launeau, P., Barillé, L., Rincé, Y., 2003. Cartographie des peuplements du microphytobenthos par télédétection spatiale visible-infrarouge dans un écosystème conchylicole. 326, pp. 377–389. https://doi.org/10.1016/S1631-0691(03)00125-2.
Méléder, V., Savelli, R., Barnett, A., Polsenaere, P., Gernez, P., Cugier, P., Lerouxel, A., Le Bris, A., Dupuy, C., Le Fouest, V., Lavaud, J., 2020. Mapping the intertidal microphytobenthos gross primary production part I: coupling multispectral remote sensing and physical modeling. Front. Mar. Sci. 7, 1–16. https://doi.org/10.3389/fmars.2020.00520.
Migné, A., Spilmont, N., Davoult, D., 2004. In situ measurements of benthic primary production during emersion: seasonal variations and annual production in the bay of Somme (eastern English Channel, France). Cont. Shelf Res. 24, 1437–1449. https://doi.org/10.1016/j.csr.2004.06.002.
Morris, J.T., 2006. Competition among marsh macrophytes by means of geomorphological displacement in the intertidal zone. Estuar. Coast. Shelf Sci. 69, 395–402. https://doi.org/10.1016/j.ecss.2006.05.025.
Morris, E.P., Peralta, G., Benavente, J., Freitas, R., Rodrigues, A.M., Quintino, V., Alvarez, O., Valcárcel-pérez, N., 2009. Caulerpa prolifera stable isotope ratios reveal anthropogenic nutrients within a tidal lagoon. Mar. Ecol. Prog. Ser. 390, 117–128. https://doi.org/10.3354/meps08184.
Niculescu, S., Talab Ou Ali, H., Billey, A., 2018. Random forest classification using Sentinel-1 and Sentinel-2 series for vegetation monitoring in the Pays de Brest (France). In: Neale, C.M., Maltese, A. (Eds.), Remote Sensing for Agriculture, Ecosystems, and Hydrology XX. SPIE, p. 6 https://doi.org/10.1117/12.2325546.
Oiry, S., Barillé, L., 2021. Using sentinel-2 satellite imagery to develop microphytobenthos-based water quality indices in estuaries. Ecol. Indic. 121, 107184. https://doi.org/10.1016/j.ecolind.2020.107184.
Orvain, F., Lefebvre, S., Montepini, J., Sébire, M., Gangnery, A., Sylvand, B., 2012. Spatial and temporal interaction between sediment and microphytobenthos in a temperate estuarine macro-intertidal bay. Mar. Ecol. Prog. Ser. 458, 53–68. https://doi.org/10.3354/meps09698.
Papaspyrou, S., Smith, C.J., Dong, L.F., Whitby, C., Dumbrell, A.J., Nedwell, D.B., 2014. Nitrate reduction functional genes and nitrate reduction potentials persist in deeper estuarine sediments. Why? PLoS One 9, e94111. https://doi.org/10.1371/journal.pone.0094111.
Paterson, D.M., 1989. Short-term in the erodibility of intertidal cohesive sediments related to the migratory behavior of epipelic diatoms. Limnol. Oceanogr. 34, 223–234. https://doi.org/10.2307/2837074.
Pinckney, J.L., Zingmark, R., 1991. Effects of tidal stage and sun angles on intertidal benthic microalgal productivity. Mar. Ecol. Prog. Ser. 76, 81–89. https://doi.org/10.3354/meps076081.
Pu, R., Bell, S., 2017. Mapping seagrass coverage and spatial patterns with high spatial resolution IKONOS imagery. Int. J. Appl. Earth Obs. Geoinf. 54, 145–158. https://doi.org/10.1016/j.jag.2016.09.011.
R Core Team, 2017. R: A Language and Environment for Statistical Computing. R Foundation for Statistical Computing, Vienna, Austria. https://www.R-project.org/.
Rouse, J., Hass, R.H., Schell, J.A., Deering, D.W., 1973. Monitoring vegetation systems in the great plains with ERTS. Third Earth Resour. Technol. Satell. Symp. 1, 309–317.
Sanchez De Lamadrid Rey, A., Muñoz Pérez, J.L., 1994. El medio físico y biológico en la Bahia de Cádiz: saco interior. Dirección General de Investigación, Tecnología y Formación Agroalimentaria y Pesquera. Junta de Andalucía.
Savelli, R., Dupuy, C., Barillé, L., Lerouxel, A., Guizien, K., Philippe, A., Bocher, P., Polsenaere, P., Fouest, V.Le, 2018. On biotic and abiotic drivers of the microphytobenthos seasonal cycle in a temperate intertidal mudflat: a modelling study. Biogeosciences 15, 7243–7271. https://doi.org/10.5194/bg-15-7243-2018.
Savelli, R., Méléder, V., Cugier, P., Polsenaere, P., Dupuy, C., Lavaud, J., Barnett, A., Le Fouest, V., 2020. Mapping the intertidal microphytobenthos gross primary production, part II: merging remote sensing and physical-biological coupled modeling. Front. Mar. Sci. 7, 1–15. https://doi.org/10.3389/fmars.2020.00521.
Scholz, B., Liebezeit, G., 2012. Microphytobenthic dynamics in a Wadden Sea intertidal flat – part II: seasonal and spatial variability of non-diatom community components in relation to abiotic parameters. Eur. J. Phycol. 47, 120–137. https://doi.org/10.1080/09670262.2012.665251.

Sen2Cor, Sen2Cor (version2.8) Sentinel Application Platform (SNAP) toolbox [software] http://step.esa.int/main/third-party-plugins-2/sen2cor/ European Space Agency (ESA).

Serôdio, J., Catarino, F., 2000. Modelling the primary productivity of intertidal microphytobenthos: time scales of variability and effects of migratory rhythms. Mar. Ecol. Prog. Ser. 192, 13–30. https://doi.org/10.3354/meps192013.

Serôdio, J., Vieira, S., Cruz, S., Barroso, F., 2005. Short-term variability in the photosynthetic activity of microphytobenthos as detected by measuring rapid light curves using variable fluorescence. Mar. Biol. 146, 903–914. https://doi.org/10.1007/s00227-004-1504-6.

Serôdio, J., Coelho, H., Vieira, S., Cruz, S., 2006. Microphytobenthos vertical migratory photoresponse as characterised by light-response curves of surface biomass. Estuar. Coast. Shelf Sci. 68, 547–556. https://doi.org/10.1016/j.ecss.2006.03.005.

Serôdio, J., Cartaxana, P., Coelho, H., Vieira, S., 2009. Effects of chlorophyll fluorescence on the estimation of microphytobenthos biomass using spectral reflectance indices. Remote Sens. Environ. 113, 1760–1768. https://doi.org/10.1016/j.rse.2009.04.003.

St-Pierre, A.P., Gagnon, P., 2020. Kelp-bed dynamics across scales: enhancing mapping capability with remote sensing and GIS. J. Exp. Mar. Bio. Ecol. 522, 151246. https://doi.org/10.1016/j.jembe.2019.151246.

Traganos, D., Reinartz, P., 2018. Interannual change detection of mediterranean seagrasses using RapidEye image time series. Front. Plant Sci. 9, 1–15. https://doi.org/10.3389/fpls.2018.00096.

Ubertini, M., Lefebvre, S., Gangnery, A., Grangeré, K., Le Gendre, R., Orvain, F., 2012. Spatial variability of benthic-pelagic coupling in an estuary ecosystem: consequences for microphytobenthos resuspension phenomenon. PLoS One 7, e44155. https://doi.org/10.1371/journal.pone.0044155.

Underwood, G.J.C., 2001. Microphytobenthos. Encyclopedia of Ocean Sciences. Elsevier, pp. 1770–1777 https://doi.org/10.1006/rwos.2001.0213.

Underwood, G.J.C., Kromkamp, J., 1999. Primary production by phytoplankton and microphytobenthos in estuaries. Adv. Ecol. Res. 29, 93–153. https://doi.org/10.1016/S0065-2504(08)60192-0.

Underwood, G.J.C., Provot, L., 2000. Determining the environmental preferences of four estuarine epipelic diatom taxa: growth across a range of salinity, nitrate and ammonium conditions. Eur. J. Phycol. 35, 173–182. https://doi.org/10.1080/09670260010001735761.

Underwood, G.J.C., Smith, D.J., 1998. Predicting epipelic diatom exopolymer concentrations in intertidal sediments from sediment chlorophyll a. Microb. Ecol. 35, 116–125. https://doi.org/10.1007/s002489900066.

Underwood, G.J.C., Paterson, D.M., Parkes, R.J., 1995. The measurement of microbial carbohydrate exopolymers from intertidal sediments. Limnol. Oceanogr. 40, 1243–1253. https://doi.org/10.4319/lo.1995.40.7.1243.

Underwood, G.J.C., Phillips, J., Saunders, K., 1998. Distribution of estuarine benthic diatom species along salinity and nutrient gradients. Eur. J. Phycol. 33, 173–183. https://doi.org/10.1080/09670269810001736673.

Van der Wal, D., Wielemaker-van den Dool, A., Herman, P.M.J., 2010. Spatial synchrony in intertidal benthic algal biomass in temperate coastal and estuarine ecosystems. Ecosystems 13, 338–351. https://doi.org/10.1007/s10021-010-9322-9.

Van der Wal, D., Van Dalen, J., Wielemaker-van den Dool, A., Dijkstra, J.T., Ysebaert, T., 2014. Biophysical control of intertidal benthic macroalgae revealed by high-frequency multispectral camera images. J. Sea Res. 90, 111–120. https://doi.org/10.1016/j.seares.2014.03.009.

Weerman, E.J., Herman, P.M.J., Van De Koppel, J., 2011. Top-down control inhibits spatial self-organization of a patterned landscape. Ecology 92, 487–495. https://doi.org/10.1890/10-0270.1.

Wilson, K.L., Skinner, M.A., Lotze, H.K., 2019. Eelgrass (Zostera marina) and benthic habitat mapping in Atlantic Canada using high-resolution SPOT 6/7 satellite imagery. Estuar. Coast. Shelf Sci. 226, 106292. https://doi.org/10.1016/j.ecss.2019.106292.

Yallop, M.L., de Winder, B., Paterson, D.M., Stal, L.J., 1994. Comparative structure, primary production and biogenic stabilization of cohesive and non-cohesive marine sediments inhabited by microphytobenthos. Estuar. Coast. Shelf Sci. 39, 565–582. https://doi.org/10.1016/S0272-7714(06)80010-7.

Zhang, T., Tian, B., Wang, Y., Liu, D., Sun, S., Duan, Y., Zhou, Y., 2021. Quantifying seasonal variations in microphytobenthos biomass on estuarine tidal flats using Sentinel-1/2 data. Sci. Total Environ. 777, 146051. https://doi.org/10.1016/j.scitotenv.2021.146051.

Zoffoli, L.M., Gernez, P., Rosa, P., Le, A., Brando, V.E., Barillé, A., Harin, N., Peters, S., Poser, K., Spaias, L., Peralta, G., Barillé, L., 2020. Remote sensing of environment Sentinel-2 remote sensing of zostera noltei-dominated intertidal seagrass meadows. Remote Sens. Environ. 251, 112020. https://doi.org/10.1016/j.rse.2020.112020.